RESEARCH ARTICLE

BJP | BRITISH PHARMACOLOGICAL SOCIETY

Endothelial AMPKα1/PRKAA1 exacerbates inflammation in HFD-fed mice

Qiuhua Yang[1] | Qian Ma[1,2] | Jiean Xu[1,2] | Zhiping Liu[1,3] | Xiaoxiao Mao[1,2] | Yaqi Zhou[2] | Yongfeng Cai[2] | Qingen Da[4] | Mei Hong[2] | Neal L. Weintraub[1] | David J. Fulton[1] | Eric J. Belin de Chantemèle[1] | Yuqing Huo[1]

[1]Vascular Biology Center, Department of Cellular Biology and Anatomy, Medical College of Georgia, Augusta University, Augusta, Georgia, USA

[2]State Key Laboratory of Chemical Oncogenomics, Key Laboratory of Chemical Genomics, Peking University, Shenzhen, China

[3]Guangdong Province Key Laboratory of Pharmacodynamic Constituents of Traditional Chinese Medicine and New Drugs Research, College of Pharmacy, Jinan University, Guangzhou, China

[4]Department of Cardiovascular Surgery, Peking University Shenzhen Hospital, Shenzhen, China

Correspondence
Yuqing Huo, Vascular Biology Center, Department of Cellular Biology and Anatomy Medical College of Georgia, Augusta University, Augusta, GA 30912, USA.
Email: yhuo@augusta.edu

Funding information
American Heart Association, Grant/Award Number: 19TPA34910043; National Institutes of Health, Grant/Award Numbers: R01EY030500, R01HL134934

Background and Purpose: Excess nutrient-induced endothelial cell inflammation is a hallmark of high fat diet (HFD)-induced metabolic syndrome. Pharmacological activation of the protein kinase AMP-activated α1 (PRKAA1) also known as AMPKα1, shows its beneficial effects in many studies of cardiometabolic disorders. However, AMPKα1, as a major cellular sensor of energy and nutrients in endothelial cells, has not been studied for its physiological role in excess nutrient-induced endothelial cell (EC) inflammation.

Experimental Approach: Wild-type and EC-specific *Prkaa1* knockout mice were fed with an HFD. Body weight, fat mass composition, glucose, and lipid levels were monitored regularly. Insulin sensitivity was analysed systemically and in major metabolic organs/tissues. Inflammation status in metabolic organs/tissues were examined with quantitative RT-PCR and flow cytometry. Additionally, metabolic status, inflammation severity, and signalling in cultured ECs were assayed with multiple approaches at the molecular level.

Key Results: EC *Prkaa1* deficiency unexpectedly alleviated HFD-induced metabolic syndromes including decreased body weight and fat mass, enhanced glucose clearance and insulin sensitivity, and relieved adipose inflammation and hepatic steatosis. Mechanistically, *PRKAA1* knockdown in cultured ECs reduced endothelial glycolysis and fatty acid oxidation, decreased levels of acetyl-CoA and suppressed transcription

of inflammatory molecules mediated by ATP citrate lyase and histone acetyltransferase p300.

Conclusions and Implications: This unexpected pro-inflammatory effect of endothelial AMPKα1/PRKAA1 in a metabolic context provides additional insight in AMPKα1/PRKAA1 activities. An in-depth study and thoughtful consideration should be applied when AMPKα1/PRKAA1 is used as a therapeutic target in the treatment of metabolic syndrome.

KEYWORDS
AMPKA1/PRKAA1, endothelial cells, inflammation, metabolism

1 | INTRODUCTION

Metabolic syndrome is characterized by central obesity combined with dyslipidaemia, hypertension, insulin resistance, and chronic low-grade inflammation, and it affects all age groups worldwide and is associated with high rates of morbidity and mortality (de Ferranti & Mozaffarian, 2008; Grundy et al., 2005; Sharma, 2011). Endothelial inflammation precedes the onset of metabolic syndrome in diet-induced obesity and insulin resistance (Graupera & Claret, 2018). Inflamed endothelium of the vessel wall recruits circulating leukocytes including monocytes, T-cells, and neutrophils to metabolic organs and tissue (Grandl & Wolfrum, 2018). The infiltrated leukocytes first initiate and then accelerate inflammation, interfering with insulin sensitivity of metabolic cells, such as adipocytes, hepatocytes, and skeletal muscle cells, resulting in the development of metabolic syndrome (Bai & Sun, 2015).

Endothelial cell metabolism, especially glycolysis and fatty acid oxidation (FAO), is an important regulator in directing the fate of endothelial cells and their activities. A growing body of evidence indicates that endothelial cell metabolism is markedly perturbed in pathologies such as atherosclerosis, pulmonary hypertension, lung sepsis, and other diseases (Cao et al., 2019; Wang et al., 2019; Yang et al., 2018). Glycolysis is the main energy source of endothelial cells, which provides 75–85% of the ATP required for endothelial cell homeostasis maintenance and proliferation (Quintero et al., 2006) and increased glycolysis is accompanied with elevation of inflammation in diseased endothelial cells (Feng et al., 2017; Wu et al., 2017). FAO-derived **acetyl coenzyme A** (acetyl-CoA) is essential for histone acetylation of lymphatic genes and retains the identity of endothelial cells by reducing the TGFβ-induced endothelial to mesenchymal transition (EndMT) (Wong et al., 2017; Xiong et al., 2018). FAO also plays an important role in sustaining the tricarboxylic acid (TCA) cycle for redox homeostasis through the regeneration of NADPH (Kalucka et al., 2018). It is unclear whether and how glycolysis and FAO in endothelial cells regulate endothelial inflammation in the context of excessive levels of nutrients.

The AMP-activated protein kinase (AMPK) is an important energy sensor and metabolic regulator in energy homeostasis (Hardie et al., 2012). AMPK is a serine/threonine kinase composed of one

What is already known

- AMPKα1, a major cellular sensor of energy, is a pharmacological target in metabolic syndrome treatment.
- Endothelial inflammation plays an important role in the development of obesity and insulin resistance.

What does this study add

- Endothelial *AMPKα1/PRKAA1* knockdown reduces palmitate-induced endothelial inflammation.
- Endothelial-specific *Prkaa1* deficiency suppresses high fat diet-induced obesity and insulin resistance.

What is the clinical significance

- These results warrant a careful consideration when AMPKα1/PRKAA1 is used as a pharmacological target.

catalytic subunit α and two regulatory subunits β and γ, each with a unique tissue distribution (Hardie & Carling, 1997; Hardie et al., 2003). **PRKAA1/AMPKα1** is the predominant isoform in vascular cells and macrophages, and **PRKAA2/AMPKα2** is the major catalytic isoform in liver, muscle, and hypothalamus (Fisslthaler & Fleming, 2009; Towler & Hardie, 2007). AMPK is activated by many cellular stresses such as exercise, hypoxia, and oxidative stress. Activated AMPK regulates several key metabolic enzymes and phosphorylates downstream kinases by switching off biosynthetic pathways and switching on catabolic pathways to maintain whole-body energy homeostasis of the cells (Hardie, 2004). A large body of research work has demonstrated that AMPK is a therapeutic target for the treatment of cardiometabolic diseases, including Type 2 diabetes and obesity. The activator of AMPK, metformin, is one of the most commonly used drugs for the treatment of Type 2 diabetes (Davis et al., 2006). However, the effect of AMPK activation is complex. Sustained activation of AMPK signalling

enhances the production of pro-inflammatory cytokines and subsequently regulates systemic inflammation and cardiometabolic diseases (Foretz et al., 2005; Liang et al., 2014). The role of endothelial PRKAA1/AMPKα1 in excess nutrient-induced endothelial cell inflammation and HFD-induced metabolic syndrome remains undefined.

This study was aimed at determining the effect of endothelial PRKAA1/AMPKα1 in endothelial inflammation and HFD-induced metabolic syndrome. We found that selective deficiency of *Prkaa1* in endothelial cells (*Prkaa1*$^{\Delta VEC}$) attenuated HFD-induced weight gain, insulin resistance, adiposity, and hepatic steatosis in mice. Our in vitro study showed that excess nutrients activate PRKAA1/AMPKα1 in endothelial cells, increase glycolysis and FAO, elevate acetyl-CoA production, and up-regulate histone acetylation via ATP citrate lyase (ACLY) and the histone acetyltransferase p300, eventually promoting endothelial inflammation. These results demonstrate a critical role of endothelial cell PRKAA1/AMPKα1 in linking endothelial metabolism, epigenetic modulation and endothelial inflammation in the development of metabolic syndrome.

2 | METHODS

2.1 | Animals

All animal care and experimental procedures complied with the National Institutes of Health Guide for the Care and Use of Laboratory Animals and relevant ethical regulations, and were approved by the Institutional Animal Care & Use Committee of Augusta University. Welfare-related assessments, measurements and interventions were carried out before, during, and after the experiment. Animal studies are reported in compliance with the ARRIVE guidelines (Percie du Sert et al., 2020) and with the recommendations made by the *British Journal of Pharmacology* (Lilley et al., 2020).

Prkaa1-floxed mice were kindly provided by Dr. Benoit Viollet (Institut Cochin, Paris, France). *Prkaa1*$^{\Delta VEC}$ mice were generated by crossing *Prkaa1*$^{f/f}$ with *Cdh5*^{Cre} transgenic mice (006137; The Jackson Laboratory; RRID:IMSR_JAX:006137) as previously described (Yang et al., 2018). All mice were genotyped by PCR amplification of tail-clip samples (Table S1). Experiments were performed with both male and female mice, and littermates were used as controls. Mice were housed in temperature-controlled cages under a 12-h light–dark cycle and given free access to water and normal chow diet (CD) or high fat diet (HFD, D12492, Research Diet, New Brunswick, NJ, USA). All mice used in this study were on a C57BL/6J background. *Prkaa1*^{WT} and *Prkaa1*$^{\Delta VEC}$ female and male mice were fed with HFD for 12 weeks beginning at the age of 6 weeks. Body weight was measured weekly and metabolic parameters were recorded with Comprehensive Lab Animal Monitoring System (CLAMS) at 10 weeks of HFD, followed by glucose tolerance test (GTT), insulin tolerance test (ITT), and nuclear magnetic resonance (NMR) at 11 or 12 weeks of HFD. Mice were killed (i.p. injection of ketamine 100 mg kg^{-1} and xylazine 10 mg kg^{-1}, followed by cervical dislocation) after 12 weeks of HFD, and major metabolic organs or tissues were harvested and processed for further analyses. Researchers were blinded to the assignment of diet and evaluation of the experimental outcomes.

2.2 | Metabolic evaluation

GTT and ITT were performed as described previously (Xu et al., 2019). In brief, for GTT, 6-h fasted mice were injected i.p. with D-glucose (1 g·kg^{-1}), and blood samples were collected and measured at 0, 30, 60, 90, and 120 min after glucose injection. For ITT, 4-h fasted mice were given insulin (1 U·kg^{-1}), and blood samples were collected and measured at the same time points as GTT with a glucometer (OneTouch UltraEasy, Johnson & Johnson). Body composition of mice was assessed by NMR (MiniSpec LF90II TD-NMR Analyzer). Oxygen consumption (VO$_2$), carbon dioxide production (VCO$_2$), food intake, and heat production were monitored with CLAMS (Columbus Instruments). At the end of HFD administration, mice were anaesthetised with ketamine (80 mg·kg^{-1}) and xylazine (5 mg·kg^{-1}), given i.p.. Mice were fasted for 12–14 h before blood was collected. Individual kits were purchased from Thermo Scientific for measuring serum concentrations of cholesterol, triglyceride, and glucose (#TR15421, TR13421, and TR22421; Thermo Scientific). The content of hepatic triglyceride was determined using tissue lipids extracted by a mixture of chloroform and methanol as previously described (Xu et al., 2019).

2.3 | Adipose stromal vascular fraction isolation and flow cytometry analysis

Perigonadal adipose tissue (approximately 100 mg per mouse) was excised immediately after killing and digested on a shaker at 37°C for 45 min in 10-ml DMEM medium (A14430-01; Gibco) containing 1 mg·ml^{-1} collagenase D (COLLD-RO; Sigma-Aldrich), 10 mg·ml^{-1} BSA, 0.5-mM CaCl$_2$, and 15-mM HEPES. After centrifugation at 500*g* for 5 min at 4°C, stromal vascular fraction (SVF) pellets were obtained. SVF samples were incubated in FACS buffer (0.1% BSA in PBS, pH 7.4) containing 2-μg Fc block (553141; BD Biosciences; RRID: AB_394656) for 15 min at room temperature and then stained with antibodies (Table S2) against PE anti-mouse F4/80 (565410; BD Biosciences; RRID:AB_2687527), PerCP-Cy5.5 anti-mouse CD11b (561114; BD Biosciences; RRID:AB_2033995), FITC anti-mouse CD206 (141703; Biolegend; RRID:AB_10900988), APC anti-mouse CD11c (550261; BD Biosciences; RRID:AB_398460), or isotype controls for 30 min at 4°C in the dark. Cells were then washed with 1-ml FACS buffer and then analysed with a FACSCalibur flow cytometer with CellQuest software (BD Pharmingen; RRID:SCR_014489).

2.4 | Histological analysis and liver Oil Red O staining

Mouse adipose and liver tissues were fixed in 4% PFA buffer and embedded in paraffin or OCT, and then blocks were sectioned at

5-μm thickness using a paraffin microtome or Microm cryostat. After deparaffinization and rehydration, endogenous peroxidase activity of sections was destroyed with H_2O_2 (3-ml 30% H_2O_2 in 200-ml methanol) for 30 min at room temperature, and then sections were boiled in 10-mM citrate buffer (pH 6.0) at 98°C for 10 min for antigen retrieval. Sections were blocked with avidin blocking solution with 10% rabbit serum and incubated with Mac-2 (ACL8942F; Accurate Chemical & Scientific Corporation), Icam-1 (SC-8439; Santa Cruz; RRID: AB_627123), and Vcam-1 (Ab134047; Abcam; RRID:AB_2721053) antibodies in biotin blocking solution overnight at 4°C. On the next day, sections were incubated with biotinylated secondary antibody (BA4001; Vector Laboratories; RRID:AB_10015300), followed by VECTASTAIN® ABC reagents (PK6100; Vector Laboratories) for 30 min at room temperature and DAB solution. Whole-amount isolectin GS-IB4 staining in adipose tissue was performed with a protocol described previously (Xu et al., 2019), the numbers of adipogenic/angiogenic cell clusters (AACCs) in distal epididymal adipose tissue from one mouse were determined by an observer blinded to the conditions, and the number of AACCs in control group was normalized to 1. Oil Red O staining of liver was performed in frozen tissue, and lipid accumulation was quantified via measuring Oil Red O staining using Image-Pro Plus software (Media Cybemetics; RRID:SCR_007369).

2.5 | Cell culture and siRNA/adenovirus infection of human umbilical vein endothelial cells

Primary human umbilical vein endothelial cells (HUVECs) were purchased from the ATCC (PCS-100-013™) and cultured with Vascular Cell Basal Medium (PCS-100-030™; ATCC) supplemented with Microvascular Endothelial Cell Growth Kit-BBE (PCS-110-040™; ATCC) in a humidified incubator with 5% CO_2 at 37°C. siRNA /adenovirus infection of HUVECs was performed as previously described (Yang et al., 2018). HUVECs were transfected at 70% confluence with siRNA targeting human *PRKAA1* (PRKAA1 siRNA [si*PRKAA1*], sc-29673; Santa Cruz Biotechnology) or non-targeting negative control (Control siRNA [si*CTRL*], sc-37007; Santa Cruz Biotechnology), human *ACLY* (*ACLY* siRNA [si*ACLY*], L-004915-00-0005; Dharmacon), human *EP300* (*EP300* siRNA [si*EP300*], L-003486-00-0005; Dharmacon), or non-targeting negative control (Control siRNA [si*CTRL*], D-001810-10-05; Dharmacon) using Lipofectamine RNAiMax reagent (13778-150; Invitrogen) according to the manufacturer's protocols. The details are provided in Table S5.

Adenovirus infection of HUVECs was performed as previously described (Yang et al., 2018). Human PRKAA1 adenovirus (Ad-*PRKAA1*) and negative control adenovirus (Ad-*CTRL*) were kindly provided by Dr. Minghui Zou (Georgia State University, USA). HUVECs were infected at 60–70% confluence with 500-μl basal medium containing Ad-*CTRL* or Ad-*PRKAA1* adenovirus for 2 h, followed by replacing with fresh complete cell medium for a continuous culture. These cells were treated as indicated and collected for quantitative RT-PCR, western blot and monocyte adhesion assays (see below).

2.6 | Quantitative real time-PCR

Total RNA of HUVECs or tissues were collected in Trizol reagent (15596018; Invitrogen) and extracted according to the manufacturer's protocol. The cDNA was generated using iScript cDNA synthesis kit (170-8891; Bio Rad). Real-time PCR analysis was performed with Power SYBR Green PCR Master Mix (4367659; Life Technologies) by a StepOne Plus system (Applied Biosystems). 18S (human/mouse) ribosomal RNA was used as an internal control. The relative difference was expressed as the fold matched control values calculated with the efficiency-corrected $2^{-\triangle\triangle CT}$ method. The primer list for quantitative RT-PCR is provided in Table S3.

2.7 | Western blot

HUVECs (2-3×10⁶ cells in 100 μl lysis buffer) and mouse tissues (1 mg in 10 μl lysis buffer) were lysed with RIPA lysis buffer (Sigma) supplemented with 1% protease (05892970001; Roche) and 1% phosphatase inhibitors (04906845001; Roche) for 10 min on ice, and protein concentration was measured by BCA Protein Assay Kit. Samples (10-20 μg protein) were loaded and separated by 10% SDS-PAGE, electrotransferred to nitrocellulose (NC) filter membrane, and incubated with specific antibodies against p-PRKA, PRKAA1, ICAM-1, VCAM-1, ACLY, Ac-H3K9, Ac-H3K27, Ac-H3, H3, p-Akt^{Ser473}, Akt, p300, GAPDH, and β-actin. The antibodies used are provided in Table S4. Images were taken with the CheminDoc MP System (Bio Rad) and viewed by Image J software (National Institutes of Health; RRID:SCR_003070) for data analysis. The levels of targeted protein were quantitated relative to GAPDH or β-actin in the same sample and normalized to the particular control group that was randomly set as one-fold.

2.8 | Monocyte adhesion assay

Monocyte adhesion assays were performed according to protocols described previously (Wang et al., 2019). HUVECs (1∼1.5×10⁶ cells per well) were cultured with Vascular Cell Complete Medium (2 mL per well) in six-well flat-bottom plates to 60-70% confluence and then incubated in 1 mL per well of Vascular Cell Basal Medium with a mixture of 100 μl Basal Medium containing 5 μl siRNA and 100 μl Basal Medium containing 5 μl RNAiMax was added to each well of a six-well plate. The cells were incubated with this mixture for 4 h at 37 °C, which was then replaced with Vascular Cell Complete Medium (2 ml per well) for 24 h, followed by incubation with palmitate (0.4 mM) for another 24 h. After removing palmitate by washing, THP-1 cells labelled with Calcein-AM (354216; Corning) were added to the confluent monolayer of HUVECs. After 30 min of incubation, non-adherent cells were removed by washing three times with cell medium followed by fixing with 4% PFA. Fluorescent-positive cells were counted with Image J and normalized with total cell numbers of HUVECs.

For the experiments with HUVECs overexpressing PRKAA1, HUVECs (1∼1.5 x 10⁶ cells) were cultured with Vascular Cell

Complete Medium (2 ml per well) in six-well plates. Cells were infected at 60–70% confluence with 500 μl basal medium containing Ad-CTRL or Ad-PRKAA1 adenovirus (1 μl per well) for 2 h, followed by replacing with fresh complete cell medium (2 ml per well) for 24 h, followed by incubation with palmitate (0.4 mM) for another 24 h. As HUVECs were infected with GFP-expressing adenovirus, THP-1 cells were not labelled with Calcein-AM, and these unlabelled cells were added into the confluent monolayer of HUVECs. After 30 min of incubation, non-adherent THP-1 cells were removed by washing three times with cell medium followed by fixing with 4% PFA. Adherent THP-1 cells were visualized by investigators and marked with green by Photoshop program in collected images. These adherent THP-1 cells were counted with Image J, and monocyte adhesion was calculated with a method used in our previous studies (Xu et al., 2017).

2.9 | Acetyl-CoA measurement

The amount of acetyl-CoA in HUVECs was determined using Acetyl-Coenzyme A Assay Kit (MAK039; Sigma-Aldrich) according to the manufacturer's instructions.

2.10 | Extracellular acidification rate (ECAR) measurement

As described in a previous publication (Cao et al., 2019), HUVECs were infected with Ad-CTRL or Ad-PRKAA1 for 48 h, and then seeded onto Seahorse XF96 culture plates at a density of 15,000 cells per well and incubated overnight in a humidified incubator of 5% CO_2 at 37°C. On the second day, the medium was changed to XF Base Medium supplemented with 2-mM glutamine, pH adjusted to 7.4 with 0.1-M NaOH, and then the plate was incubated in a non-CO_2 incubator at 37°C for 1 h. ECAR was measured with an XF96 Extracellular Flux Analyzer (Seahorse Bioscience). Inhibitors and activators used in the test are glucose (10 mM), oligomycin (1 μM), and 2-deoxyglucose (50 mM).

2.11 | Fatty acid oxidation rate measurement

FAO was measured with XF FAO assay (102720-100; Agilent Technologies) using an XF96 Extracellular Flux Analyzer. For measuring FAO, siCTRL and siPRKAA1 pretreated HUVECs were seeded in the XF96 cell culture microplates overnight at a density of 15,000 cells per well. Cells were then incubated with FAO assay media (Krebs–Henseleit buffer supplemented with 2.5-mM glucose, 0.5-mM carnitine, and 5-mM HEPES on the day of the assay, adjusted to pH 7.4 at 37°C) for 30–45 min in a non-CO_2 incubator at 37°C, following by adding Etomoxir (40 μM) for 15 min before the assay. Palmitate-BSA FAO Substrate or BSA was added to the appropriate wells immediately before starting the assay with injections of oligomycin (2 μM), FCCP (2 μM), and antimycin A/rotenone (1 μM). The XF Cell Mito Stress Test was run according to the manufacturer's instruction.

2.12 | Data and statistical analysis

The experimental design and analysis comply with the recommendations and requirements of the British Journal of Pharmacology (Curtis et al., 2018). All studies were designed, where possible, to generate groups of equal size using randomization and blinded analysis. The immuno-related procedures used comply with the recommendations made by the British Journal of Pharmacology (Alexander et al., 2018). Some results were normalized to the control so as to avoid unwanted sources of variation. Statistical tests were performed using GraphPad Prism software (Version 8.0, RRID:SCR_000306), and all results are expressed as mean ± SEM. No outliers were identified in reported experiments, and no data were excluded from analyses. Statistical analysis was only undertaken for studies where each group size n was at least 5. Studies with n less than 5 were not subjected to statistical analysis and the related results were referred to as preliminary. Group size (n) represents the number of studied animals (in vivo) or independent values (in vitro), and statistical analysis was performed using these independent values. The statistical calculations were performed by one-way ANOVA followed by Bonferroni's post hoc tests for multiple comparisons if F reached $P < 0.05$ and there was no significant variance inhomogeneity. Student's t test was used for comparing two groups. For all comparisons, $P < 0.05$ was accepted to indicate a statistically significant difference.

2.13 | Materials

2-deoxyglucose, oligomycin, FCCP, rotenone and antimycin A were supplied as components of the Seahorse XF Glycolytic Rate Assay Kit from Agilent (Santa Clara, CA). Palmitate was supplied by Sigma-Aldrich (St. Louis, MO); ketamine and xylazine were supplied byPhoenix Scientific (St. Joseph, MO).

2.14 | Nomenclature of targets and ligands

Key protein targets and ligands in this article are hyperlinked to corresponding entries in the IUPHAR/BPS Guide to PHARMACOLOGY (http://www.guidetopharmacology.org) and are permanently archived in the Concise Guide to PHARMACOLOGY 2021/22 (Alexander, Cidlowski et al., 2021; Alexander, Fabbro et al., 2021).

3 | RESULTS

3.1 | Endothelial cell Prkaa1 deficiency improves HFD-induced systemic insulin sensitivity

To investigate the role of endothelial PRKAA1 in energy homeostasis in mice, we took advantage of an endothelial cell-specific Prkaa1 knockout (Prkaa1$^{\Delta VEC}$) mouse that we generated previously (Yang et al., 2018). Then we examined whether endothelial cell Prkaa1

deficiency could affect metabolic parameters in mice fed with a chow diet (CD, 10% kcal from fat). We did not find any difference in body weight, fat and lean content, GTT and ITT between the two groups of mice of either gender (Figures S1 and S2), indicating that the loss of endothelial cell *Prkaa1* does not make a difference in mouse whole body metabolism on CD.

We further challenged these mice with a high-fat diet (HFD, 60% kcal from fat) to investigate whether endothelial PRKAA1 plays a role in HFD-induced metabolic syndrome. *Prkaa1*$^{\Delta VEC}$ and *Prkaa1*^{WT} female and male mice were fed with HFD beginning at 6 weeks of age for 12 weeks and followed with measurement of relative metabolic parameters at time points as indicated in Section 2. On an HFD, *Prkaa1*$^{\Delta VEC}$ mice of both genders exhibited decreased body weight compared with *Prkaa1*^{WT} (Figures 1a and S3A). In addition, *Prkaa1*$^{\Delta VEC}$ mice showed a higher lean content and a lower fat content than littermate control mice (Figures 1b and S3B). Also, *Prkaa1*$^{\Delta VEC}$ mice exhibited improved systemic insulin sensitivity, as demonstrated by GTT and ITT assays (Figures 1c,d and S3C,D). Furthermore, Western blot analysis with samples of major metabolic organs/tissues from these mice showed increased levels of p-Akt^{Ser473} in adipose tissue, liver, and muscle from HFD-fed *Prkaa1*$^{\Delta VEC}$ mice stimulated by insulin, compared with those of littermate controls (Figures 1e–g and S3E-G, for group with $n < 5$, results are preliminary). Consistent with the above results, *Prkaa1*$^{\Delta VEC}$ mice had increases in oxygen consumption and carbon dioxide production without changes in food intake and respiratory exchange ratio compared with *Prkaa1*^{WT} mice after 12 weeks of HFD (Figures S4 and S5). Taken together, these results suggest that endothelial cell *Prkaa1* deficiency improved HFD-induced systemic insulin sensitivity.

3.2 | Endothelial cell *Prkaa1* deficiency ameliorates HFD-induced adipose inflammation

Growing evidence indicates that adipose tissue plays an important role in regulating metabolic homeostasis, and adipose inflammation contributes a major part in the development of HFD-induced metabolic syndrome. We examined sections of white adipose tissue (WAT) histologically with haematoxylin and eosin (H&E) staining and found that the size of adipocytes was much smaller in WAT from HFD-fed *Prkaa1*$^{\Delta VEC}$ mice than littermate controls (Figures 2a and S6A). To determine whether endothelial cell PRKAA1 regulates adipose inflammation, we performed immunostaining on adipose sections with antibody against the macrophage marker Mac2. Staining with Mac2 antibody showed that macrophage infiltration in WAT of HFD-fed *Prkaa1*$^{\Delta VEC}$ mice was much less than that of HFD-fed *Prkaa1*^{WT} mice (Figures 2b and S6B). We also performed flow cytometry analysis to quantify macrophage populations in adipose stromal vascular fractions (SVFs) of HFD-fed *Prkaa1*$^{\Delta VEC}$ and *Prkaa1*^{WT} mice. SVFs from *Prkaa1*$^{\Delta VEC}$ mice contained smaller proportions of CD11b$^+$F4/80$^+$ macrophages, fewer M1-like CD11b$^+$F4/80$^+$CD11c$^+$ cells and more M2-like CD11b$^+$F4/80$^+$CD206$^+$ cells, and a decreased ratio of M1-like to M2-like cells compared with those from *Prkaa1*^{WT} mice

(Figures 2c and S6C). Furthermore, in concordance with FACS analysis, the mRNA level of F4/80 was decreased in adipose of HFD-fed *Prkaa1*$^{\Delta VEC}$ mice compared with that of control mice (Figures 2d and S6D). Additionally, expression of several genes associated with inflammation (*Icam1*, *Vcam1*, *Ccl2*, *Il1b* and *Il6*) was reduced in WAT *of Prkaa1*$^{\Delta VEC}$ mice compared with that of controls (Figures 2e and S6E). Immunostaining of adipose sections also showed that protein levels of ICAM-1 and VCAM-1 in WAT of HFD-fed *Prkaa1*$^{\Delta VEC}$ mice were much lower than those of HFD-fed *Prkaa1*^{WT} mice (Figure 2f,g). Immunostaining of whole mount adipose tissue with isolectin GS-IB4 showed no significant difference in adipogenic/angiogenic cell cluster (AACC) number and vascular density in WAT between HFD-fed *Prkaa1*$^{\Delta VEC}$ mice and HFD-fed *Prkaa1*^{WT} mice (Figures 2h and S6F). These results suggest that, in the context of HFD feeding, endothelial PRKAA1 regulates the inflammatory state of WAT but not angiogenesis and contributes to the development of insulin resistance and fat gain.

3.3 | Endothelial cell *Prkaa1* deficiency attenuates HFD-induced hepatic steatosis and inflammation

To determine whether endothelial PRKAA1 plays a role in hepatic steatosis, sections of livers from these mice were subjected to H&E and Oil Red O staining. Lower levels of hepatic necrosis and lipid deposition were observed in sections of HFD-fed *Prkaa1*$^{\Delta VEC}$ mice than those of *Prkaa1*^{WT} mice (Figures 3a,b and S7A,B). Decreased lipid accumulation in the liver was further confirmed by direct triglyceride measurement (Figures 3c and S7C). Consistent with these data, much lower mRNA levels of the genes related to fatty acid synthesis (*Fasn*) and FAO (*Pparg* and *Cpt1a*) assayed with qRT-PCR were observed in the livers of HFD-fed *Prkaa1*$^{\Delta VEC}$ mice than HFD-fed *Prkaa1*^{WT} mice (Figures 3d and S7D).

Mac2 staining of liver sections showed less macrophage infiltration into livers of HFD-fed *Prkaa1*$^{\Delta VEC}$ mice than *Prkaa1*^{WT} mice (Figures 3e and S7E). This is in line with the F4/80 mRNA levels in livers of the two groups of mice, assessed by qRT-PCR (Figures 3f and S7F). The expression of CD206 (a marker of anti-inflammatory M2 macrophages) was increased in livers of HFD-fed *Prkaa1*$^{\Delta VEC}$ mice compared with *Prkaa1*^{WT} mice (Figures 3f and S7F). The inflammatory status of livers in these mice was further examined. Compared with HFD-fed *Prkaa1*^{WT} mice, *Prkaa1*$^{\Delta VEC}$ mice showed a significant decrease in the mRNA levels of iNOS, and proinflammatory cytokines including *Ccl2*, *Tnfa*, and *Il1b* were much lower in livers of HFD-fed *Prkaa1*$^{\Delta VEC}$ mice than those of HFD-fed *Prkaa1*^{WT} mice (Figures 3f and S7F). We further examined mRNA levels of *Pecam-1*, *Cdh5*, *Icam-1*, and *Vcam-1* in livers of mice. The expression of *Pecam-1* and *Cdh5* was increased while the expression of *Icam-1* and *Vcam-1* was decreased in liver samples of HFD-fed *Prkaa1*$^{\Delta VEC}$ mice compared with that in HFD-fed *Prkaa1*^{WT} mice (Figures 3g and S7G). Immunostaining also showed that protein levels of Icam-1 and Vcam-1 in liver of HFD-fed *Prkaa1*$^{\Delta VEC}$ mice was reduced compared with that of HFD-fed *Prkaa1*^{WT} mice
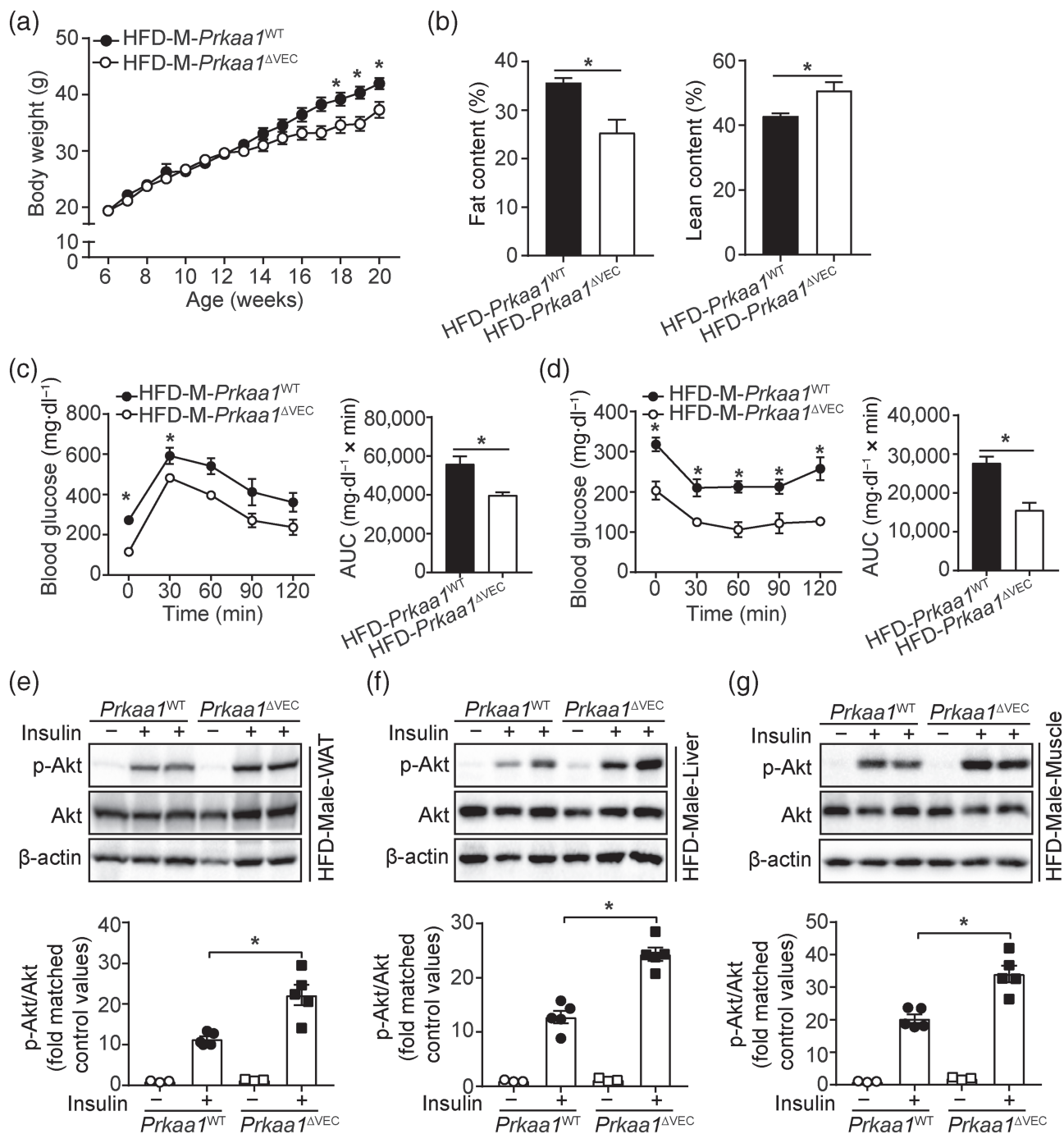
FIGURE 1 Endothelial cell *Prkaa1* deficiency improves HFD-induced systemic insulin sensitivity. (a) Body weight of *Prkaa1*[WT] and *Prkaa1*[ΔVEC] male mice during 12 weeks of HFD. $n = 9$. (b) Fat and lean content of *Prkaa1*[WT] and *Prkaa1*[ΔVEC] male mice after 12 weeks of HFD. $n = 9$. (c) Blood glucose level during the glucose tolerance test (GTT) and calculated areas under curve (AUC) of GTT in *Prkaa1*[WT] and *Prkaa1*[ΔVEC] male mice after 10 weeks of HFD. $n = 6$. (d) Blood glucose level during the insulin tolerance test (ITT) and calculated AUC of ITT in *Prkaa1*[WT] and *Prkaa1*[ΔVEC] male mice after 11 weeks of HFD. $n = 6$. (e–g) Western blot analysis of p-Akt (Ser473), total Akt, and β-actin from epididymal WAT, liver, and quadriceps muscle in *Prkaa1*[WT] and *Prkaa1*[ΔVEC] male mice after 12 weeks of HFD. Samples were collected from mice after injection with saline or insulin (1 U·kg^{-1}) for 5 min into the inferior vena cava. The quantification of p-Akt/total Akt were analysed by densitometry of Western blot. $n = 3$ per saline group, $n = 5$ per insulin group. Data are presented as the mean ± SEM. *$P < 0.05$, significant difference between *Prkaa1*[WT] and *Prkaa1*[ΔVEC]; unpaired Student's *t* test

(Figure 3h,i), indicating the preserved endothelial integrity and decreased inflammatory response in endothelial cells in livers of HFD-*Prkaa1*[ΔVEC] mice. Collectively, these results indicate that

endothelial *Prkaa1* deficiency decreases endothelial inflammation, reduces macrophage infiltration into liver and, consequently, attenuates HFD-induced hepatic steatosis.
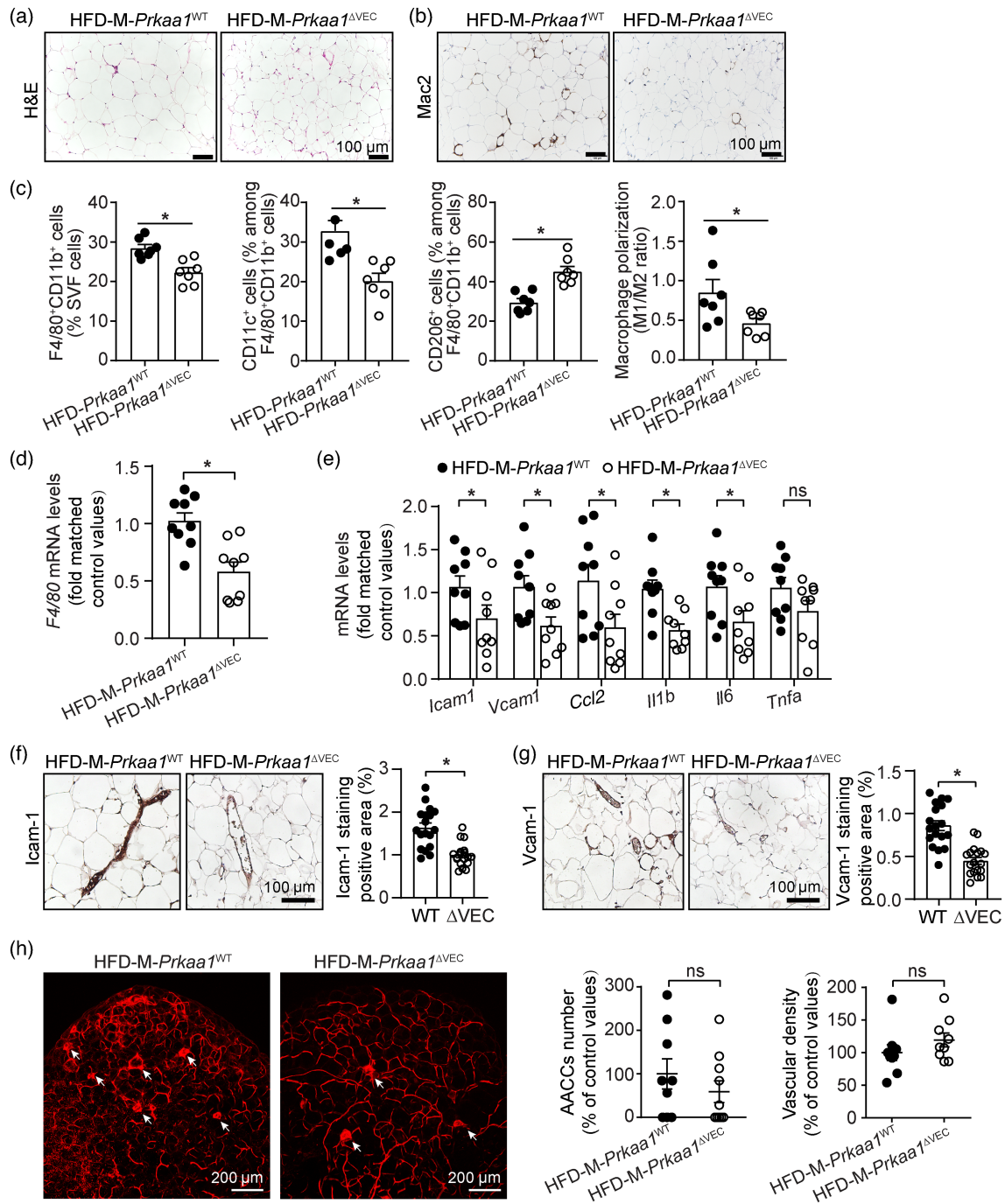
FIGURE 2 Endothelial cell *Prkaa1* deficiency ameliorates HFD-induced adipose inflammation. (a) Representative image of haematoxylin and eosin (H&E) staining of adipose tissue sections from *Prkaa1*[WT] and *Prkaa1*[ΔVEC] male mice after 12 weeks of HFD. (b) Representative image of Mac2 staining of adipose tissue sections from *Prkaa1*[WT] and *Prkaa1*[ΔVEC] male mice after 12 weeks of HFD. (c) Flow cytometry analysis of the percentage of F4/80^{+}CD11b^{+} macrophages among stromal vascular fraction (SVF), F4/80^{+}CD11b^{+}CD11c^{+} (M1) macrophages, percentage of F4/80^{+}CD11b^{+}CD206^{+} (M2) macrophages, and the ratio of M1 to M2 macrophages from *Prkaa1*[WT] and *Prkaa1*[ΔVEC] male mice after 12 weeks of HFD. $n = 7$. (d) Quantitative RT-PCR analysis of the mRNA level of *F4/80* in adipose tissue from *Prkaa1*[WT] and *Prkaa1*[ΔVEC] male mice after 12 weeks of HFD. $n = 9$ mice per group. (e) Quantitative RT-PCR analysis of the mRNA level of *Icam1*, *Vcam1*, *Ccl2*, *Tnfa*, *Il1b*, and *Il6* in adipose tissue from *Prkaa1*[WT] and *Prkaa1*[ΔVEC] male mice after 12 weeks of HFD. $n = 9$ mice per group. (f, g) Representative images and summary data of ICAM-1 and VCAM-1 staining of adipose sections of *Prkaa1*[WT] and *Prkaa1*[ΔVEC] male mice after 12 weeks of HFD. Three areas per mouse and six mice per group were collected and quantified. (h) Representative images of immunofluorescence staining for isolectin GS-IB4 and quantification data of adipogenic/angiogenic cell cluster (AACC) numbers, as indicated by arrows, and vessel density in epididymal WAT of *Prkaa1*[WT] and *Prkaa1*[ΔVEC] male mice after 12 weeks of HFD. $n = 9$ mice per group. Data are presented as the mean ± SEM. *$P < 0.05$, significantly different as indicated; ns: not significantly different; unpaired Student's *t* test
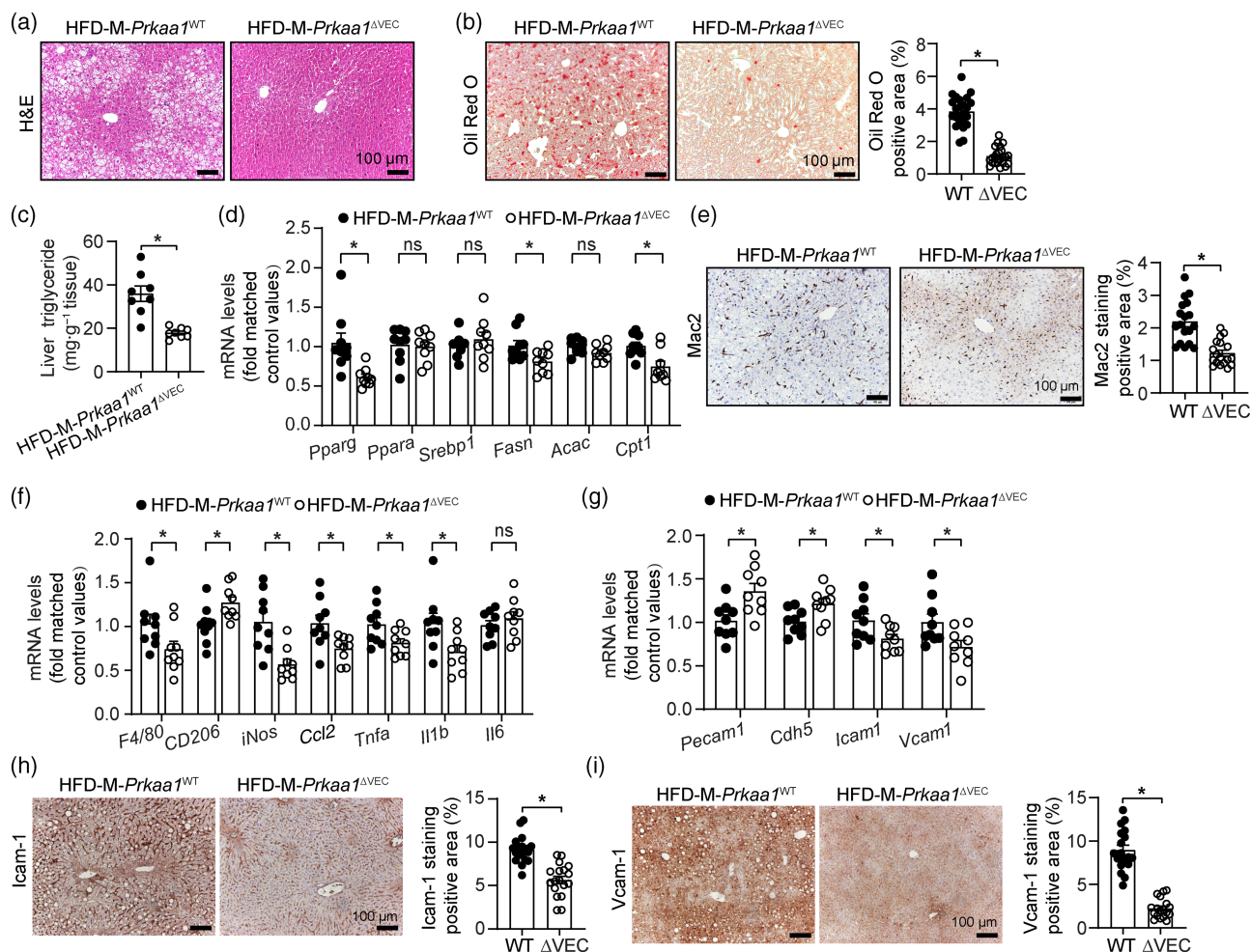
FIGURE 3 Endothelial cell *Prkaa1* deficiency attenuates HFD-induced hepatic steatosis and inflammation. (a) Representative images of haematoxylin and eosin (H&E) staining of liver sections from *Prkaa1*^WT and *Prkaa1*^ΔVEC male mice after 12 weeks of HFD. (b) The representative images and quantification data of Oil Red O staining of liver sections from *Prkaa1*^WT and *Prkaa1*^ΔVEC male mice after 12 weeks of HFD. Four areas per mice and six mice per group were collected and quantified. (c) Liver triglyceride levels of *Prkaa1*^WT and *Prkaa1*^ΔVEC male mice after 12 weeks of HFD. $n = 8$ mice per group. (d) Quantitative RT-PCR analysis of the mRNA level of *Pparg*, *Ppara*, *Srbp1*, *Fasn*, *Acac*, and *Cpt1* in liver from *Prkaa1*^WT and *Prkaa1*^ΔVEC male mice after 12 weeks of HFD. $n = 9$ mice per group. (e) Representative images and summary data of Mac2 staining of liver sections from *Prkaa1*^WT and *Prkaa1*^ΔVEC male mice after 12 weeks of HFD. Three areas per mouse and six mice per group were collected and quantified. (f) Quantitative RT-PCR analysis of the mRNA level of *F4/80*, *CD206*, *iNos*, *Ccl2*, *Tnfa*, *Il1b*, and *Il6* in liver from *Prkaa1*^WT and *Prkaa1*^ΔVEC male mice after 12 weeks of HFD. $n = 9$ mice per group. (g) Quantitative RT-PCR analysis of the mRNA level of *Pecam1*, *Cdh5*, *Icam1*, and *Vcam1* in liver from *Prkaa1*^WT and *Prkaa1*^ΔVEC male mice after 12 weeks of HFD. $n = 9$ mice per group. (h, i) Representative images and summary data of ICAM-1 and VCAM-1 staining of liver sections from *Prkaa1*^WT and *Prkaa1*^ΔVEC male mice after 12 weeks of HFD. Three areas per mouse and six mice per group were collected and quantified. All data were presented as mean ± SEM. *$P < 0.05$, significantly different as indicated; ns, not significantly different as indicated; unpaired Student's t test

3.4 | The absence of *PRKAA1* decreases palmitate-induced endothelial cell inflammation

As the in vivo data indicated a decreased endothelial inflammation in endothelial *Prkaa1*-deficient mice, we next investigated whether PRKAA1 contributed to endothelial inflammation in in vitro assays. Increased circulating levels of fatty acids including palmitate are a major feature of the excessive nutrients in mice fed with a HFD (Nakamura et al., 2009). We therefore exposed HUVECs to palmitate in order to determine the influence of metabolic stress on the expression of PRKAA1. Incubation with palmitate up-regulated the mRNA

level of *PRKAA1* in HUVECs in a dose- and time-dependent manner (Figure 4a). Treatment with palmitate also led to up-regulation of p-PRKA^T172 and PRKAA1 at the protein level (Figure 4b). The up-regulated PRKA expression and activation by palmitate were accompanied by increased expression of adhesion molecules such as ICAM-1 and VCAM-1, indicating a possible association of palmitate-stimulated PRKAA1 with increased endothelial inflammation.

To determine whether PRKAA1 contributes to palmitate-stimulated endothelial inflammation, we further assessed the mRNA levels of inflammatory molecules of PA-treated HUVECs transfected with si*CTRL* or si*PRKAA1* by quantitative RT-PCR analysis. The results
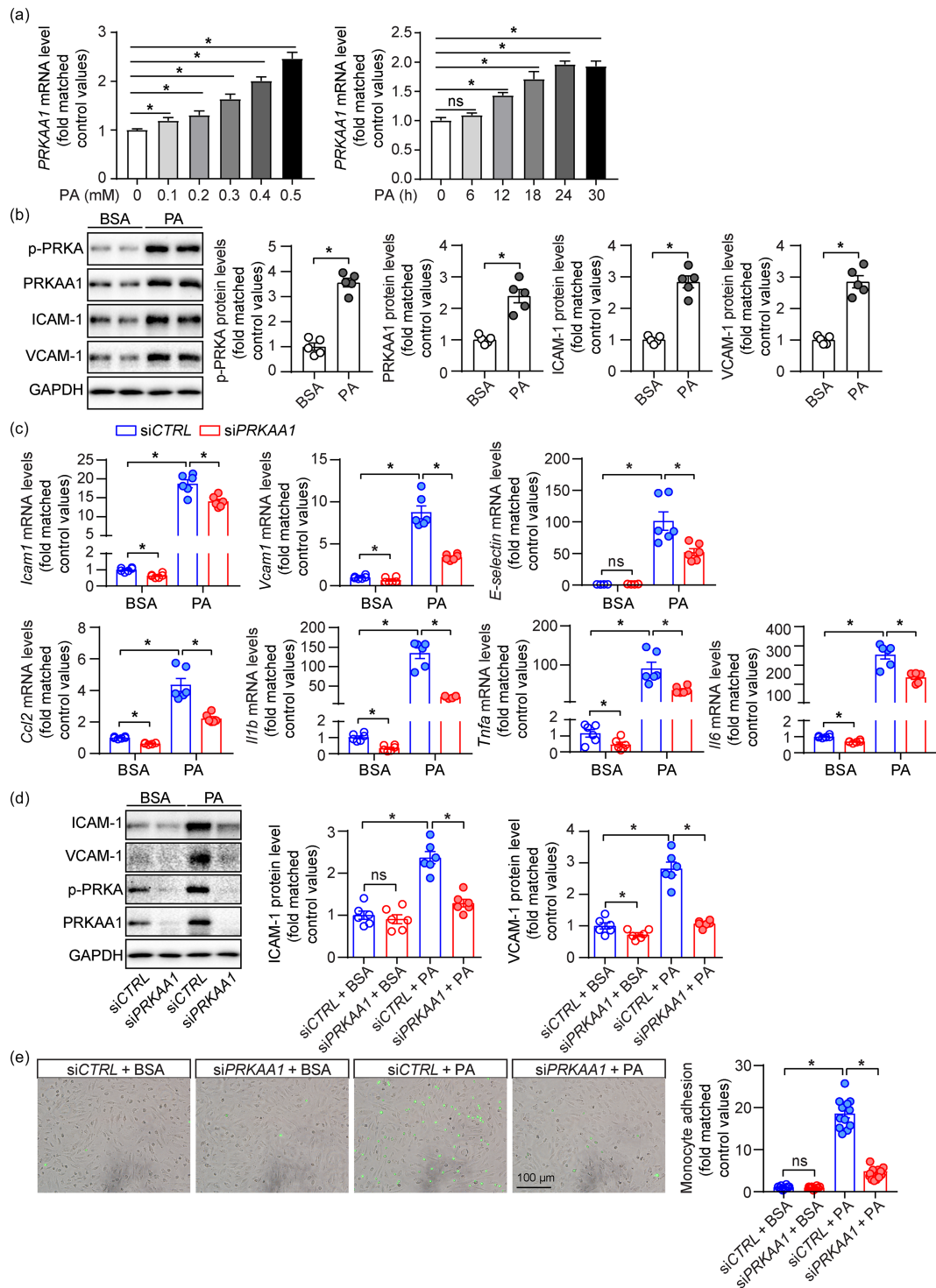
FIGURE 4 The absence of *PRKAA1* decreases palmitate-induced endothelial cell inflammation. (a) (Left) Quantitative RT-PCR analysis of mRNA level of *PRKAA1* in HUVECs treated with increasing concentrations of palmitate (PA; 0.1–0.5 mM) for 24 h. $n = 6$. (Right) Quantitative RT-PCR analysis of mRNA level of *PRKAA1* in HUVECs treated with palmitate (PA; 0.4 mM) for 0, 6, 12, 18, 24, and 30 h. $n = 6$. (b) Western blot analysis and densitometric quantification of the protein levels of p-PRKA, PRKAA1, ICAM-1, and VCAM-1 in HUVECs treated with palmitate (PA; 0.4 mM) or vehicle for 24 h. $n = 5$. (c) Quantitative RT-PCR analysis of the mRNA levels of *Icam1*, *Vcam1*, *E-selectin*, *Ccl2*, *Il1b*, *Tnfa* and *Il6* in HUVECs transfected with si*PRKAA1* or si*CTRL* for 24 h, followed with palmitate (PA; 0.4 mM) or BSA treatment for another 24 h. $n = 6$. (d) Western blot analysis and densitometric quantification of the protein levels of ICAM-1, VCAM-1, p-PRKA, PRKAA1, and GAPDH in HUVECs transfected with si*PRKAA1* or si*CTRL* for 24 h, followed with palmitate (PA; 0.4 mM) or BSA treatment for another 24 h. $n = 6$. (e) Representative images and summary data of monocyte adhesion to HUVECs transfected with si*PRKAA1* or si*CTRL* for 24 h, followed with palmitate (PA; 0.4 mM) or BSA treatment for another 24 h. $n = 12$. All data were presented as mean ± SEM. *$P < 0.05$, significantly different as indicated, ns: not significantly different as indicated; unpaired Student's *t* test (b) or one-way ANOVA followed by Bonferroni test (a, c, d, and e)

showed that the mRNA levels of *ICAM-1*, *VCAM-1*, *E-selectin*, *Ccl2*, *Ilb*, *Tnfa*, and *Il6* were decreased in HUVECs transfected with si*PRKAA1* compared with those of control cells upon palmitate treatment (Figure 4c). Western blot analysis revealed that exposure to palmitate markedly induced the expression of adhesion molecules (ICAM-1 and VCAM-1); these effects induced by palmitate were attenuated in *PRKAA1* knockdown HUVECs compared with control HUVECs (Figure 4d). Furthermore, we found that the palmitate-induced increased adhesiveness of HUVECs to THP-1 monocytic cells was reduced when HUVECs were transfected with si*PRKAA1* (Figure 4e). All together, these findings indicate that the absence of *PRKAA1* in HUVECs reduces palmitate-induced expression of inflammatory molecules and endothelial adhesiveness to monocytes.

3.5 | The overexpression of *PRKAA1* increases PA-induced endothelial cell inflammation

Following examination of PRKAA1 for endothelial inflammation by a loss-of-function approach, we investigated this effect with gain-of-function, which is overexpression of PRKAA1 in HUVECs. We infected HUVECs with adenovirus encoding constitutively active PRKA mutant (Ad-*PRKAA1*) and control adenovirus (Ad-*CTRL*) and processed these cells for inflammation assays. Compared with HUVECs infected with Ad-*CTRL*, HUVECs with overexpression of *PRKAA1* expressed high mRNA levels of inflammatory cytokines (*ICAM-1*, *VCAM-1*, *E-selectin*, *Ccl2*, *Il1b*, *Tnfa*, and *Il6*) in the presence of either BSA or palmitate (Figure 5a). In addition, Western blots showed that the protein levels of ICAM-1 and VCAM-1 were higher in HUVECs infected with Ad-*PRKAA1* than those cells with Ad-*CTRL* (Figure 5b). Accordingly, palmitate treatment increased endothelial adhesiveness to monocytes, and this effect was significantly exaggerated in HUVECs infected with Ad-*PRKAA1* compared with control cells (Figure 5c,d). Taken together, these results suggest that overexpression of *PRKAA1* enhances palmitate-stimulated inflammatory actions in endothelial cells.

3.6 | The absence or overexpression of *PRKAA1* influences endothelial inflammation by altering the endothelial metabolism via the ACLY-EP300 pathway

Having shown that knockdown of *PRKAA1* decreased endothelial cell glycolysis in our previous work (Yang et al., 2018), we next sought to determine whether overexpression of *PRKAA1* increases glycolysis. Using Seahorse Extracellular Flux analysis, we assessed glycolytic metabolism in *PRKAA1*-overexpressing HUVECs via measurement of the extracellular acidification rate (ECAR). As shown in Figure 6a, overexpression of *PRKAA1* exhibited significantly increased glycolysis and glycolytic capacity, compared with control cells. Furthermore, we also examined the effect of PRKAA1 on regulation of FAO. For this end, we performed Seahorse assays with *PRKAA1* knockdown HUVECs to determine the OCR in the presence of palmitate. As

shown in Figure 6b, FAO was dramatically decreased in *PRKAA1* knockdown HUVECs compared with control cells, indicating a critical role of PRKAA1 in FAO. We then explored whether PRKAA1-regulated metabolism contributes to acetyl-CoA production. The results showed that *PRKAA1* knockdown decreased and *PRKAA1* overexpression increased acetyl-CoA production in HUVECs at baseline, and under palmitate treatment, respectively, compared with control cells (Figure 6c,d). Acetyl-CoA is a substrate of protein acetylation, and we postulated that the change of acetyl-CoA production regulated by PRKAA1 might affect protein acetylation. Indeed, Western blot showed that the protein levels of the acetylated histones, Ac-H3K9, Ac-H3K27, and Ac-H3, were enhanced in palmitate-treated cells; this effect was abolished by *PRKAA1* knockdown in HUVECs (Figure 6e).

It has been reported that increased acetylation epigenetically up-regulates expression of inflammatory molecules (Rafehi et al., 2015). The enzyme ATP citrate lyase (ACLY) metabolizes citrate to acetyl-CoA for protein acetylation, and p300 acts as an acetyltransferase to acetylate transcriptional factors to increase transcription of adhesion molecules (Shen et al., 2017; Wellen et al., 2009). To demonstrate whether PRKAA1 regulates palmitate-induced endothelial cell inflammation via the acetylation pathway, *PRKAA1*-overexpressed HUVECs were treated with siRNA of *ACLY* or *EP300* under palmitate treatment, and the protein levels of adhesion molecules were evaluated with Western blot. As shown in Figure 6f,g, the increased protein levels of ICAM-1 and VCAM-1 in *PRKAA1*-overexpressing HUVECs were markedly reduced by si*ACLY* and si*EP300*. These results suggest that PRKAA1 increases endothelial glycolysis and FAO, enhances the levels of acetyl-CoA and, eventually, affects transcription of inflammatory molecules through ACLY and EP300-associated acetylation.

4 | DISCUSSION

Our study has uncovered the effect of endothelial PRKAA1/AMPKα1 in regulating endothelial cell metabolism in the presence of excess nutrients. Excess nutrients increased the expression and activity of endothelial PRKAA1/AMPKα1. Such enhanced AMPKα1 up-regulated endothelial cell metabolism including glycolysis and FAO, increased acetyl-CoA production and, consequently, increased the transcription of inflammatory molecules via an epigenetic pathway. Deficiency of endothelial *Prkaa1/AMPKα1* protected mice from HFD-induced endothelial inflammation, macrophage infiltration into metabolic organs and tissues and the development of metabolic syndrome (Figure 7).

Endothelial cell *Prkaa1*/AMPKα1 deficiency unexpectedly protected mice from the development of HFD-induced metabolic syndrome. PRKAA1/AMPKα1 exists as an energy sensor and metabolic regulator, and its activation exhibits a number of beneficial effects on metabolic and cardiovascular diseases. A769662, metformin, and AICAR have been regarded as activators of AMPK activators and they exhibit protection against obesity and the related metabolic syndrome (Buhl et al., 2002; Cheang et al., 2014; Wu et al., 2018). The role of AMPK in metabolic organs and tissues in improving metabolic function has
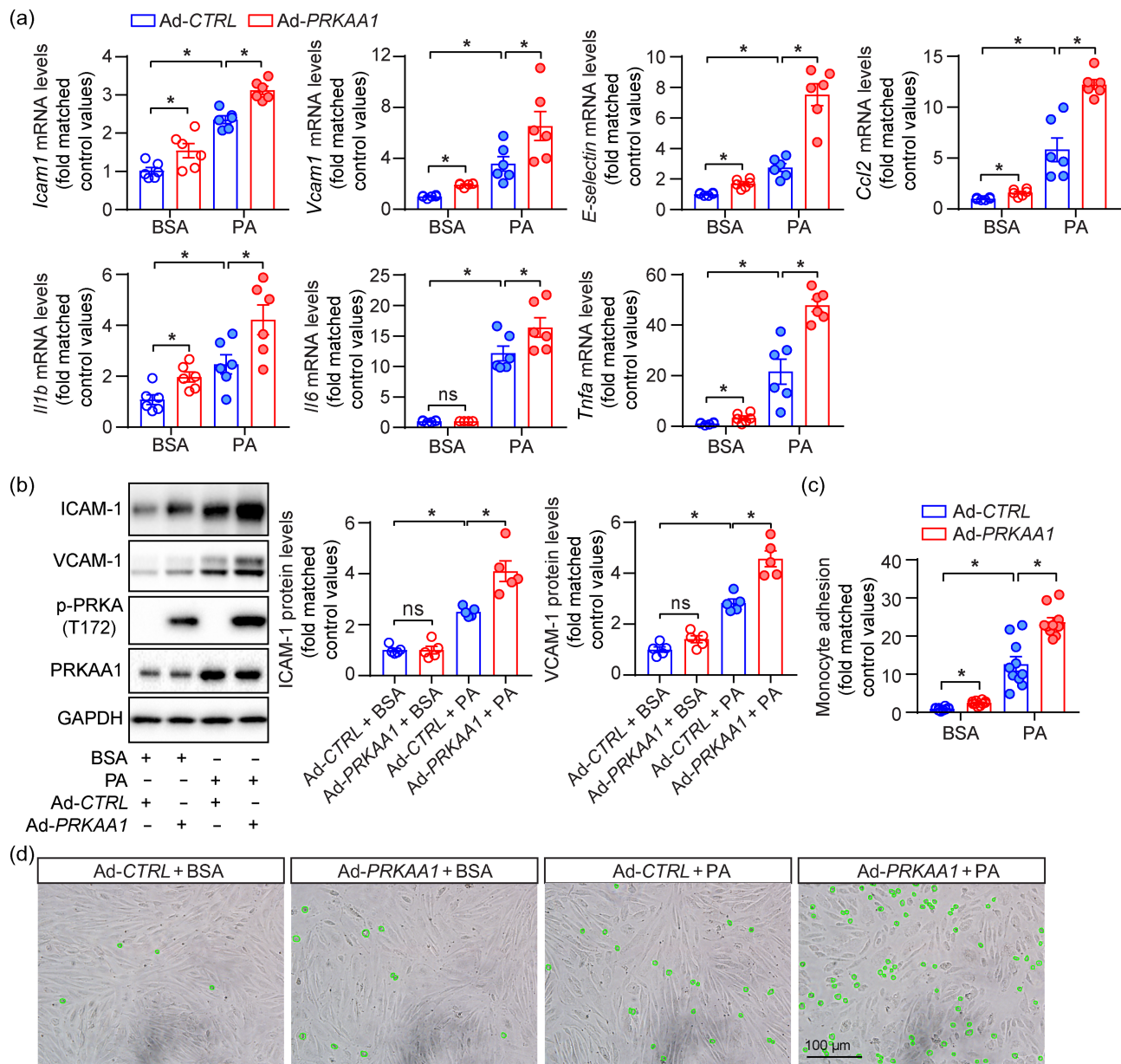
FIGURE 5 The overexpression of *PRKAA1* increases palmitate-induced endothelial cell inflammation. (a) Quantitative RT-PCR analysis of the mRNA levels of *Icam1*, *Vcam1*, *E-selectin*, *Ccl2*, *Il1b*, *Il6*, and *Tnfa* in HUVECs infected with Ad-*PRKAA1* or Ad-*CTRL* for 24 h, followed with palmitate (PA; 0.4 mM) or BSA treatment for another 24 h. $n = 6$. (b) Western blot analysis and densitometric quantification of the protein levels of ICAM-1, VCAM-1, p-PRKA, PRKAA1, and GAPDH in HUVECs infected with Ad-*PRKAA1* or Ad-*CTRL* for 24 h, followed with palmitate (PA; 0.4 mM) or BSA treatment for another 24 h. $n = 5$. (c, d) Summary data (c) and representative images (d) of monocyte adhesion to HUVECs infected with Ad-*PRKAA1* or Ad-*CTRL* for 24 h, followed with palmitate (PA; 0.4 mM) or BSA treatment for another 24 h. $n = 12$. All data were presented as mean ± SEM. *$P < 0.05$, significantly different as indicated, ns: not significantly different as indicated; one-way ANOVA followed by Bonferroni test

also been well established in a genetic model. Genetic deletion of AMPKα1/α2 in adipose tissue increased HFD-induced adiposity and aggravated hepatic steatosis and impaired glucose tolerance and insulin sensitivity (Wu et al., 2018). Also, another study showed that deficiency of both the AMPK β1 and β2 subunits in adipocytes exhibited more HFD-induced hepatic steatosis as well as glucose and insulin intolerance (Mottillo et al., 2016). In addition to adipose tissue, genetic liver-specific AMPK activation showed reduced liver steatosis and

diet-induced obesity by reprograming lipid metabolism (Garcia et al., 2019). However, the effects of endothelial AMPK in cardiometabolic diseases are less clear-cut. One group reported that selective endothelial AMPK activation mobilized endothelial progenitor cells (EPCs) and enhanced incorporation of EPCs into injured blood vessels in mice (Li et al., 2012). In contrast, another set of results showed that constitutive activation of endothelial AMPKα1 promoted HFD-induced liver injury and inflammatory responses
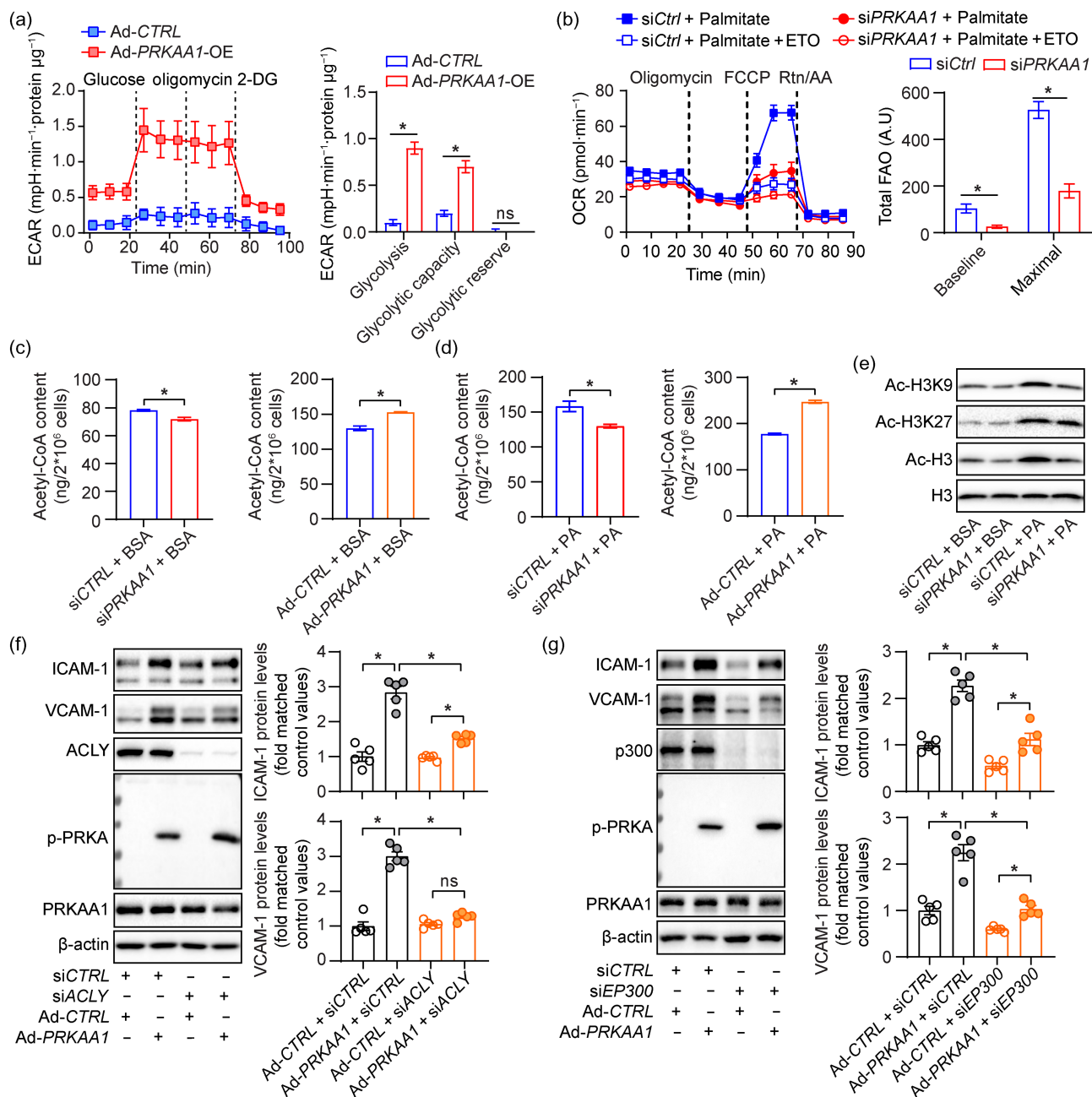
FIGURE 6 Metabolic alteration of HUVECs in the presence or overexpression of *PRKAA1* with palmitate treatment. (a) (Left) ECAR profile showing glycolytic activity in HUVECs infected with Ad-*PRKAA1* or Ad-*CTRL* for 48 h. Vertical lines represent the time of injected glucose (10 mM), oligomycin (1 μM), and 2-deoxyglucose (2-DG; 50 mM). (Right) Quantification data of glycolytic function parameters. (For all panels: $n = 8$ per group; replicated three times). (b) (Left) OCR profile showing total FAO in HUVECs transfected with si*PRKAA1* or si*CTRL* for 48 h with BSA-palmitate. Etomoxir (ETO, 40 μM) was added to some wells 15 min before the assay. Vertical lines represent the time of injected oligomycin (2 μM), FCCP (2 μM), and antimycin A (AA) /rotenone (1 μM). (Right) Quantification of total FAO as the difference between conditions with or without etomoxir treatment, both containing BSA-palmitate. (For all panels: $n = 8$ per group; replicated three times). (c) The content of acetyl-CoA in HUVECs infected with si*PRKAA1* or si*CTRL* or Ad-*PRKAA1* or Ad-*CTRL* for 48 h. $n = 6$. (d) The content of acetyl-CoA in HUVECs infected with si*PRKAA1* or si*CTRL* or Ad-*PRKAA1* or Ad-*CTRL* for 24 h, followed with palmitate (PA; 0.4 mM) treatment for another 24 h. $n = 6$. (e) Western blot analysis of the protein levels of Ac-H3K9, Ac-H3K27, Ac-H3, and H3 in HUVECs transfected with si*PRKAA1* or si*CTRL* for 24 h, followed with palmitate (PA; 0.4 mM) or BSA treatment for another 24 h. $n = 5$. (f) Western blot analysis and densitometric quantification of the protein levels of ICAM-1, VCAM-1, ACLY, p-PRKA, PRKAA1, and β-actin in HUVECs infected with Ad-*CTRL*-si*CTRL*, Ad-*PRKAA1*-si*CTRL*, Ad-*CTRL*-si*ACLY*, and Ad-*PRKAA1*-si*ACLY* with palmitate (PA; 0.4 mM) treatment for 24 h. $n = 5$. (g) Western blot analysis and densitometric quantification of the protein levels of ICAM-1, VCAM-1, p-PRKA, PRKAA1, and β-actin in HUVECs infected with Ad-*CTRL*-si*CTRL*, Ad-*PRKAA1*-si*CTRL*, Ad-*CTRL*-si*EP300*, and Ad-*PRKAA1*-si*EP300* with palmitate (PA; 0.4 mM) treatment for 24 h. $n = 5$. All data were presented as mean ± SEM. *$P < 0.05$, significantly different as indicated, ns: not significantly different as indicated; unpaired Student's t test (a–d) or one-way ANOVA followed by Bonferroni test (f, g)
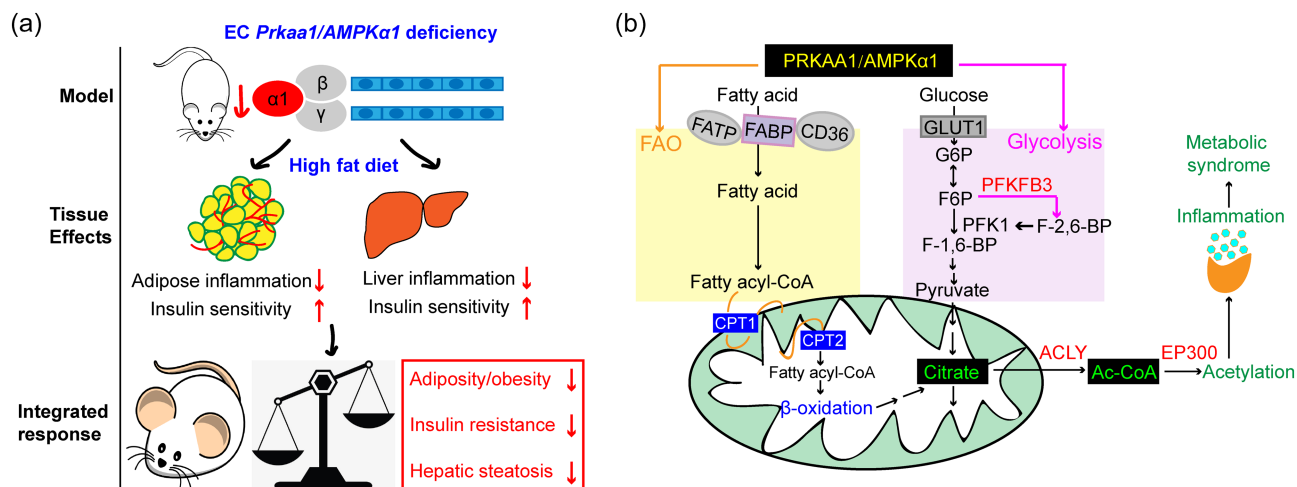
FIGURE 7 Schematic diagram illustrating the effects and mechanisms of endothelial cell (EC) *Prkaa1/AMPKα1* deficiency in mice on HFD-induced metabolic syndrome. Deficiency of EC *Prkaa1/AMPKα1* protects mice from HFD-induced endothelial inflammation, macrophage infiltration into metabolic organs/tissue, and the development of metabolic syndrome. Mechanistically, excess nutrients increase expression and activity of endothelial PRKAA1/AMPKα1. The enhanced AMPKα1 up-regulates EC metabolism including glycolysis and FAO, increases acetyl-CoA production and, consequently, drives the transcription of inflammatory molecules via an epigenetic pathway

(Liang et al., 2014). Consistent with the latter study, our study has demonstrated that genetic deletion of endothelial AMPKα1/PRKAA1 protects against HFD-induced inflammatory responses and insulin resistance in metabolic organs and tissues.

Previous studies have reported that the activation of AMPK suppresses inflammation induced by different stimuli. AMPK activators, such as AICAR, metformin, A-769662, and **adenine**, inhibit inflammatory responses stimulated by TNFα and **lipopolysaccharide (LPS).** Metformin and AICAR suppress **IKK** phosphorylation and stabilize the NF-κB-IκBα complex, further attenuating TNFα-induced NF-κB activation and inflammation in vascular endothelial cells (Hattori et al., 2006; Huang et al., 2009; Zhang et al., 2011). Adenine, another activator of AMPK, also shows an inhibitory effect of TNFα-induced inflammation in HUVECs (Cheng et al., 2015). In contrast with these studies displaying the anti-inflammatory effect of AMPK activation, some studies have shown a pro-inflammatory role of the AMPK signalling pathway. Thus, constitutive activation of *Prkaa1* promoted endothelial cell inflammation and induction of **COX-2**, suggesting that the increased COX-2 expression represents a pro-inflammatory effect that offsets protective functions of AMPK activation (Liang et al., 2014). Other studies also showed that sustained activation of AMPK enhanced pro-inflammatory cytokine production by increased endothelial cell senescence and further modulated systemic inflammation (Wang et al., 2011; Zu et al., 2010). In our current study, palmitate treatment increased PRKAA1 expression in both a time- and dose-dependent manner, and knockdown of *Prkaa1* decreased the mRNA and protein levels of the adhesion molecules ICAM-1 and VCAM-1 in palmitate-activated HUVECs and also prevented monocyte adhesion to endothelial cells. Consistent with these data, genetic overexpression of *Prkaa1* by adenovirus promoted the expression of inflammatory molecules and monocyte

adhesion to endothelial cells. These divergent effects of AMPK activation on endothelial inflammation are likely to be due to the different biological and metabolic environments, indicating a context-dependent inflammatory or anti-inflammatory effect of AMPK activation in endothelial cells.

Many studies have shown that AMPK regulates whole-body energy homeostasis, such as regulating FAO and glucose uptake in heart, affecting fatty acid synthesis and cholesterol synthesis in liver, and regulating lipolysis in adipose cells (Hardie et al., 2012). AMPKα1, the major catalytic isoform in vascular endothelial cells, plays an important role in the regulation of endothelial cell metabolism. In proliferating endothelial cells, metabolism is considered to be mainly glycolysis, while in quiescent endothelial cells, it is considered to be fatty acid oxidation (De Bock et al., 2013; Kalucka et al., 2018; Xu et al., 2014). In proliferating endothelial cells, FAO sustains the TCA cycle to support nucleotide synthesis, while in quiescent endothelial cells, FAO is up-regulated to sustain the TCA cycle for redox homeostasis against oxidative stress-prone exposure (Kalucka et al., 2018; Schoors et al., 2015). Our group has elucidated the functional role of PRKAA1/AMPKα1 in regulating endothelial glycolysis and have found that PRKAA1-mediated endothelial cell glycolysis protects against the development of atherosclerosis (Yang et al., 2018). Consistent with previous work, this study further confirmed that the overexpression of *Prkaa1* increased endothelial cell glycolysis. AMPK activation increases FAO in endothelial cells (Dagher et al., 2001) and the current study also found decreased OCR in endothelial cells with *Prkaa1* knockdown. These results indicate that PRKAA1/AMPKα1 is a critical mediator of glycolysis and FAO in endothelial cells.

Endothelial cells take up nutrients and reprogram endothelial cell metabolism to support their proliferation and homeostasis. Over past years, increased attention has been focused on endothelial cell

metabolism and its regulatory role in endothelial cell dysfunction and related cardiovascular diseases, such as atherosclerosis (Yang et al., 2018), ischaemia disease (Paternotte et al., 2008), pulmonary hypertension (Cao et al., 2019), ocular diseases (Shah et al., 2013), cancer (Yeh, Lin, & Fu, 2008), and vascular aging (Toda, 2012). Glycolysis has been regarded as a regulator of endothelial cell inflammation in many inflammatory cardiovascular diseases (Soto-Heredero et al., 2020; Theodorou & Boon, 2018). 2-Deoxyglucose (2-DG), a glucose analogue that inhibits glycolysis and the expression of inflammatory molecules in endothelial cells, protects against the development of aortic aneurysm in mice (Tsuruda et al., 2012). In contrast, the enhanced glycolysis by HIF1A overexpression increases endothelial inflammation and accelerates the development of atherosclerosis in mice (Wu et al., 2017). Moreover, pro-inflammatory cytokines up-regulate endothelial cell glycolysis, which further enhances cytokine-induced NF-κB activation (Cantelmo et al., 2016). Despite a large number of studies helping to understand the relationship between endothelial cell metabolism and inflammation, there is no study on the role of endothelial metabolism in endothelial inflammation in models of the metabolic syndrome. In this study, we found that in endothelial cells, PRKAA1/AMPKα1-mediated metabolism regulated the inflammatory responses induced by excess nutrients and further affected the development of HFD-induced obesity and insulin resistance.

AMPK is a critical player in aspects of epigenetic regulation, such as histone acetylation, phosphorylation and methylation (Gongol et al., 2018). Protein acetylation is a process that transfers an acetyl group from acetyl-CoA to the ε-amino side chain of lysine residues by **histone acetyltransferases (HATs)** and **deacetylases (HDACs)** (Drazic et al., 2016). Acetyl-CoA, a key molecule in metabolism and transcription, plays an important role in regulating protein acetylation. Snf1, the homologue of AMPK in yeast, regulates the production of acetyl-CoA and global histone acetylation via phosphorylating and inhibiting the activity of **acetyl-CoA carboxylase** (Zhang et al., 2013). AMPK activation by AICAR increases the level of acetyl-CoA and subsequently increases histone acetylation by accumulated acetyl-CoA (Gongol et al., 2018). In contrast to AMPK activation, the deletion of *AMPK/PRKA* in leukaemia cells shows decreased acetyl-CoA levels and leads to decreased histone acetylation. Supplementation of acetate into cultured *AMPK*-deficient LICs restored the acetyl-CoA level and histone acetylation (Jiang et al., 2017). Acetylation of histones and other molecules such as EP300 enhances transcription of inflammatory molecules (Lan et al., 2019). In this study, the decreased inflammation in *PRKAA1/AMPKα1* knockdown endothelial cells is accompanied by a low level of acetyl-CoA. Interestingly, counteracting the increased acetyl-CoA in *PRKAA1/AMPKα1*-overexpressing cells by knockdown of *ACLY* or *EP300* reduces increased inflammation in *PRKAA1/AMPKα1*-overexpressing endothelial cells. Thus, endothelial cell PRKAA1/AMPKα1 enhances endothelial cell metabolism, elevating the acetyl-CoA level, thus promoting epigenetic transcription of inflammatory molecules and consequently promoting development of metabolic syndrome.

In conclusion, this study using endothelial cell *Prkaa1*-deficient mice and *PRKAA1*-knockdown in HUVECs demonstrates that endothelial cell AMPKα1/PRKAA1 links endothelial metabolism, epigenetic modulation and endothelial inflammation in the development of metabolic syndrome. The findings from this study indicate a complex role of AMPKα1/PRKAA1 in endothelial cells, suggesting that a careful investigation is warranted for use of AMPKα1/PRKAA1 as a therapeutic target in the treatment of metabolic disorders.

AUTHOR CONTRIBUTIONS

QY and YH conceived the study; QY, QM, and JX, proposed the method, conducted the experiments, and analysed the data; ZL, XM, YZ, YC, QD, and MH conducted the experiments and analysed the data; QY and YH wrote the manuscript; and NW, DF, and EC revised the manuscript. All authors reviewed the report and approved the final version.

CONFLICT OF INTEREST

The authors declare no conflicts of interest.

DECLARATION OF TRANSPARENCY AND SCIENTIFIC RIGOUR

This Declaration acknowledges that this paper adheres to the principles for transparent reporting and scientific rigour of preclinical research as stated in the *BJP* guidelines for Design and Analysis, Immunoblotting and Immunochemistry, and Animal Experimentation, and as recommended by funding agencies, publishers and other organisations engaged with supporting research.

DATA AVAILABILITY STATEMENT

Data available on request from the authors. The data that support the findings of this study are available from the corresponding author upon reasonable request. Some data may not be made available because of privacy or ethical restrictions.

ORCID

Qiuhua Yang https://orcid.org/0000-0002-5582-3771
Yaqi Zhou https://orcid.org/0000-0003-0615-6631

REFERENCES

Alexander, S. P., Cidlowski, J. A., Kelly, E., Mathie, A., Peters, J. A., Veale, E. L., Armstrong, J. F., Faccenda, E., Harding, S. D., Pawson, A. J., Southan, C., Davies, J. A., Coons, L., Fuller, P. J., Korach, K. S., & Young, M. J. (2021). THE CONCISE GUIDE TO PHARMACOLOGY 2021/22: Nuclear hormone receptors. *British Journal of Pharmacology*, *178*(S1), S246–S263. https://doi.org/10.1111/bph.15540

Alexander, S. P., Fabbro, D., Kelly, E., Mathie, A., Peters, J. A., Veale, E. L., Armstrong, J. F., Faccenda, E., Harding, S. D., Pawson, A. J., Southan, C., Davies, J. A., Boison, D., Burns, K. E., Dessauer, C., Gertsch, J., Helsby, N. A., Izzo, A. A., Koesling, D., ... Wong, S. S. (2021). The concise guide to pharmacology 2021/22: Enzymes. *British*

Journal of Pharmacology, 178, S313–S411. https://doi.org/10.1111/bph.15542

Alexander, S. P. H., Roberts, R. E., Broughton, B. R. S., Sobey, C. G., George, C. H., Stanford, S. C., Cirino, G., Docherty, J. R., Giembycz, M. A., Hoyer, D., Insel, P. A., Izzo, A. A., Ji, Y., MacEwan, D. J., Mangum, J., Wonnacott, S., & Ahluwalia, A. (2018). Goals and practicalities of immunoblotting and immunohistochemistry: A guide for submission to the *British Journal of Pharmacology*. *British Journal of Pharmacology*, 175, 407–411. https://doi.org/10.1111/bph.14112

Bai, Y., & Sun, Q. (2015). Macrophage recruitment in obese adipose tissue. *Obesity Reviews: An Official Journal of the International Association for the Study of Obesity*, 16, 127–136. https://doi.org/10.1111/obr.12242

Buhl, E. S., Jessen, N., Pold, R., Ledet, T., Flyvbjerg, A., Pedersen, S. B., Pedersen, O., Schmitz, O., & Lund, S. (2002). Long-term AICAR administration reduces metabolic disturbances and lowers blood pressure in rats displaying features of the insulin resistance syndrome. *Diabetes*, 51, 2199–2206. https://doi.org/10.2337/diabetes.51.7.2199

Cantelmo, A. R., Conradi, L. C., Brajic, A., Goveia, J., Kalucka, J., Pircher, A., Chaturvedi, P., Hol, J., Thienpont, B., Teuwen, L. A., Schoors, S., Boeckx, B., Vriens, J., Kuchnio, A., Veys, K., Cruys, B., Finotto, L., Treps, L., Stav-Noraas, T. E., ... Carmeliet, P. (2016). Inhibition of the glycolytic activator PFKFB3 in endothelium induces tumor vessel normalization, impairs metastasis, and improves chemotherapy. *Cancer Cell*, 30, 968–985. https://doi.org/10.1016/j.ccell.2016.10.006

Cao, Y., Zhang, X., Wang, L., Yang, Q., Ma, Q., Xu, J., Wang, J., Kovacs, L., Ayon, R. J., Liu, Z., Zhang, M., Zhou, Y., Zeng, X., Xu, Y., Wang, Y., Fulton, D. J., Weintraub, N. L., Lucas, R., Dong, Z., ... Huo, Y. (2019). PFKFB3-mediated endothelial glycolysis promotes pulmonary hypertension. *Proceedings of the National Academy of Sciences*, 116, 13394–13403. https://doi.org/10.1073/pnas.1821401116

Cheang, W. S., Tian, X. Y., Wong, W. T., Lau, C. W., Lee, S. S., Chen, Z. Y., Yao, X., Wang, N., & Huang, Y. (2014). Metformin protects endothelial function in diet-induced obese mice by inhibition of endoplasmic reticulum stress through 5′ adenosine monophosphate-activated protein kinase-peroxisome proliferator-activated receptor δ pathway. *Arteriosclerosis, Thrombosis, and Vascular Biology*, 34(4), 830–836. https://doi.org/10.1161/atvbaha.113.301938

Cheng, Y.-F., Young, G.-H., Lin, J.-T., Jang, H.-H., Chen, C.-C., Nong, J.-Y., Chen, P. K., Kuo, C. Y., Kao, S. H., Liang, Y. J., & Chen, H. M. (2015). Activation of AMP-activated protein kinase by adenine alleviates TNF-alpha-induced inflammation in human umbilical vein endothelial cells. *PLoS ONE*, 10, e0142283. https://doi.org/10.1371/journal.pone.0142283

Curtis, M. J., Alexander, S., Cirino, G., Docherty, J. R., George, C. H., Giembycz, M. A., Hoyer, D., Insel, P. A., Izzo, A. A., Ji, Y., MacEwan, D. J., Sobey, C. G., Stanford, S. C., Teixeira, M. M., Wonnacott, S., & Ahluwalia, A. (2018). Experimental design and analysis and their reporting II: Updated and simplified guidance for authors and peer reviewers. *British Journal of Pharmacology*, 175, 987–993. https://doi.org/10.1111/bph.14153

Dagher, Z., Ruderman, N., Tornheim, K., & Ido, Y. (2001). Acute regulation of fatty acid oxidation and AMP-activated protein kinase in human umbilical vein endothelial cells. *Circulation Research*, 88, 1276–1282. https://doi.org/10.1161/hh1201.092998

Davis, B. J., Xie, Z., Viollet, B., & Zou, M.-H. (2006). Activation of the AMP-activated kinase by antidiabetes drug metformin stimulates nitric oxide synthesis in vivo by promoting the association of heat shock protein 90 and endothelial nitric oxide synthase. *Diabetes*, 55, 496–505. https://doi.org/10.2337/diabetes.55.02.06.db05-1064

de Bock, K., Georgiadou, M., Schoors, S., Kuchnio, A., Wong, B. W., Cantelmo, A. R., Quaegebeur, A., Ghesquière, B., Cauwenberghs, S., Eelen, G., Phng, L. K., Betz, I., Tembuyser, B., Brepoels, K., Welti, J., Geudens, I., Segura, I., Cruys, B., Bifari, F., ... Carmeliet, P. (2013). Role of PFKFB3-driven glycolysis in vessel sprouting. *Cell*, 154, 651–663. https://doi.org/10.1016/j.cell.2013.06.037

de Ferranti, S., & Mozaffarian, D. (2008). The perfect storm: Obesity, adipocyte dysfunction, and metabolic consequences. *Clinical Chemistry*, 54, 945–955. https://doi.org/10.1373/clinchem.2007.100156

Drazic, A., Myklebust, L. M., Ree, R., & Arnesen, T. (2016). The world of protein acetylation. *Biochimica et Biophysica Acta*, 1864, 1372–1401. https://doi.org/10.1016/j.bbapap.2016.06.007

Feng, S., Bowden, N., Fragiadaki, M., Souilhol, C., Hsiao, S., Mahmoud, M., Allen, S., Pirri, D., Ayllon, B. T., Akhtar, S., Thompson, A. A. R., Jo, H., Weber, C., Ridger, V., Schober, A., & Evans, P. C. (2017). Mechanical activation of hypoxia-inducible factor 1α drives endothelial dysfunction at Atheroprone sites. *Arteriosclerosis, Thrombosis, and Vascular Biology*, 37, 2087–2101. https://doi.org/10.1161/atvbaha.117.309249

Fisslthaler, B., & Fleming, I. (2009). Activation and signaling by the AMP-activated protein kinase in endothelial cells. *Circulation Research*, 105, 114–127. https://doi.org/10.1161/circresaha.109.201590

Foretz, M., Ancellin, N., Andreelli, F., Saintillan, Y., Grondin, P., Kahn, A., Thorens, B., Vaulont, S., & Viollet, B. (2005). Short-term overexpression of a constitutively active form of AMP-activated protein kinase in the liver leads to mild hypoglycemia and fatty liver. *Diabetes*, 54, 1331–1339. https://doi.org/10.2337/diabetes.54.5.1331

Garcia, D., Hellberg, K., Chaix, A., Wallace, M., Herzig, S., Badur, M. G., Lin, T., Shokhirev, M. N., Pinto, A. F. M., Ross, D. S., Saghatelian, A., Panda, S., Dow, L. E., Metallo, C. M., & Shaw, R. J. (2019). Genetic liver-specific AMPK activation protects against diet-induced obesity and NAFLD. *Cell Reports*, 26, 192–208.e196. https://doi.org/10.1016/j.celrep.2018.12.036

Gongol, B., Sari, I., Bryant, T., Rosete, G., & Marin, T. (2018). AMPK: An epigenetic landscape modulator. *International Journal of Molecular Sciences*, 19, 3238. https://doi.org/10.3390/ijms19103238

Grandl, G., & Wolfrum, C. (2018). Hemostasis, endothelial stress, inflammation, and the metabolic syndrome. *Seminars in Immunopathology*, 40, 215–224. https://doi.org/10.1007/s00281-017-0666-5

Graupera, M., & Claret, M. (2018). Endothelial cells: New players in obesity and related metabolic disorders. *Trends in Endocrinology and Metabolism: TEM*, 29, 781–794. https://doi.org/10.1016/j.tem.2018.09.003

Grundy, S. M., Cleeman, J. I., Daniels, S. R., Donato, K. A., Eckel, R. H., Franklin, B. A., Gordon, D. J., Krauss, R. M., Savage, P. J., Smith SC Jr, Spertus, J. A., Costa, F., American Heart Association, & National Heart, Lung, and Blood Institute. (2005). Diagnosis and management of the metabolic syndrome. *Circulation*, 112, 2735–2752. https://doi.org/10.1161/CIRCULATIONAHA.105.169404

Hardie, D. G. (2004). The AMP-activated protein kinase pathway—New players upstream and downstream. *Journal of Cell Science*, 117, 5479–5487. https://doi.org/10.1242/jcs.01540

Hardie, D. G., & Carling, D. (1997). The AMP-activated protein kinase—Fuel gauge of the mammalian cell? *European Journal of Biochemistry*, 246, 259–273. https://doi.org/10.1111/j.1432-1033.1997.00259.x

Hardie, D. G., Ross, F. A., & Hawley, S. A. (2012). AMPK: A nutrient and energy sensor that maintains energy homeostasis. *Nature Reviews Molecular Cell Biology*, 13, 251–262. https://doi.org/10.1038/nrm3311

Hardie, D. G., Scott, J. W., Pan, D. A., & Hudson, E. R. (2003). Management of cellular energy by the AMP-activated protein kinase system. *FEBS Letters*, 546, 113–120. https://doi.org/10.1016/S0014-5793(03)00560-X

Hattori, Y., Suzuki, K., Hattori, S., & Kasai, K. (2006). Metformin inhibits cytokine-induced nuclear factor kappaB activation via AMP-activated protein kinase activation in vascular endothelial cells. *Hypertension (Dallas, Tex: 1979)*, 47, 1183–1188. https://doi.org/10.1161/01.hyp.0000221429.94591.72

Huang, N. L., Chiang, S. H., Hsueh, C. H., Liang, Y. J., Chen, Y. J., & Lai, L. P. (2009). Metformin inhibits TNF-alpha-induced IkappaB kinase

phosphorylation, IkappaB-alpha degradation and IL-6 production in endothelial cells through PI3K-dependent AMPK phosphorylation. *International Journal of Cardiology*, *134*, 169–175. https://doi.org/10.1016/j.ijcard.2008.04.010

Jiang, Y., Nakada, D., & Kitano, A. (2017). AMPK links metabolic regulation to epigenome modification in leukemia-initiating-cell. *Blood*, *130*, 2488–2488. https://doi.org/10.1182/blood.V130.Suppl_1.2488.2488

Kalucka, J., Bierhansl, L., Conchinha, N. V., Missiaen, R., Elia, I., Brüning, U., Scheinok, S., Treps, L., Cantelmo, A. R., Dubois, C., de Zeeuw, P., Goveia, J., Zecchin, A., Taverna, F., Morales-Rodriguez, F., Brajic, A., Conradi, L. C., Schoors, S., Harjes, U., ... Carmeliet, P. (2018). Quiescent endothelial cells upregulate fatty acid β-oxidation for vasculoprotection via redox homeostasis. *Cell Metabolism*, *28*, 881–894.e813. https://doi.org/10.1016/j.cmet.2018.07.016

Lan, F., Hu, Y., Tang, D., Cai, J., & Zhang, Q. (2019). Transcription coactivator p300 promotes inflammation by enhancing p65 subunit activation in type 2 diabetes nephropathy. *International Journal of Clinical and Experimental Pathology*, *12*, 1826–1834.

Li, F. Y. L., Lam, K. S. L., Tse, H.-F., Chen, C., Wang, Y., Vanhoutte, P. M., & Xu, A. (2012). Endothelium-selective activation of AMP-activated protein kinase prevents diabetes mellitus–induced impairment in vascular function and Reendothelialization via induction of heme oxygenase-1 in mice. *Circulation*, *126*, 1267–1277. https://doi.org/10.1161/CIRCULATIONAHA.112.108159

Liang, Y., Huang, B., Song, E., Bai, B., & Wang, Y. (2014). Constitutive activation of AMPK α1 in vascular endothelium promotes high-fat diet-induced fatty liver injury: Role of COX-2 induction. *British Journal of Pharmacology*, *171*, 498–508. https://doi.org/10.1111/bph.12482

Lilley, E., Stanford, S. C., Kendall, D. E., Alexander, S. P. H., Cirino, G., Docherty, J. R., George, C. H., Insel, P. A., Izzo, A. A., Ji, Y., Panettieri, R. A., Sobey, C. G., Stefanska, B., Stephens, G., Teixeira, M., & Ahluwalia, A. (2020). ARRIVE 2.0 and the *British Journal of Pharmacology*: Updated guidance for 2020. *British Journal of Pharmacology*, *177*, 3611–3616. https://doi.org/10.1111/bph.15178

Mottillo, E. P., Desjardins, E. M., Crane, J. D., Smith, B. K., Green, A. E., Ducommun, S., Henriksen, T. I., Rebalka, I. A., Razi, A., Sakamoto, K., Scheele, C., Kemp, B. E., Hawke, T. J., Ortega, J., Granneman, J. G., & Steinberg, G. R. (2016). Lack of adipocyte AMPK exacerbates insulin resistance and hepatic steatosis through Brown and Beige adipose tissue function. *Cell Metabolism*, *24*, 118–129. https://doi.org/10.1016/j.cmet.2016.06.006

Nakamura, S., Takamura, T., Matsuzawa-Nagata, N., Takayama, H., Misu, H., Noda, H., Nabemoto, S., Kurita, S., Ota, T., Ando, H., Miyamoto, K. I., & Kaneko, S. (2009). Palmitate induces insulin resistance in H4IIEC3 hepatocytes through reactive oxygen species produced by mitochondria. *The Journal of Biological Chemistry*, *284*, 14809–14818. https://doi.org/10.1074/jbc.M901488200

Paternotte, E., Gaucher, C., Labrude, P., Stoltz, J. F., & Menu, P. (2008). Review: Behaviour of endothelial cells faced with hypoxia. *Bio-Medical Materials and Engineering*, *18*, 295–299.

Percie du Sert, N., Hurst, V., Ahluwalia, A., Alam, S., Avey, M. T., Baker, M., Browne, W. J., Clark, A., Cuthill, I. C., Dirnagl, U., Emerson, M., Garner, P., Holgate, S. T., Howells, D. W., Karp, N. A., Lazic, S. E., Lidster, K., MacCallum, C. J., Macleod, M., ... Würbel, H. (2020). The ARRIVE guidelines 2.0: Updated guidelines for reporting animal research. *PLoS Biology*, *18*(7), e3000410. https://doi.org/10.1371/journal.pbio.3000410

Quintero, M., Colombo, S. L., Godfrey, A., & Moncada, S. (2006). Mitochondria as signaling organelles in the vascular endothelium. *Proceedings of the National Academy of Sciences*, *103*, 5379–5384. https://doi.org/10.1073/pnas.0601026103

Rafehi, H., Balcerczyk, A., Lunke, S., Kaspi, A., Ziemann, M., Harikrishnan, K. N., Okabe, J., Khurana, I., Ooi, J., Khan, A. W., du, X., Chang, L., Haviv, I., Keating, S., Karagiannis, T., & el-Osta, A. (2015). Regulation of inflammatory gene expression by histone acetylation

and HDAC inhibition in human aortic endothelial cells. *Atherosclerosis*, *241*, e6. https://doi.org/10.1016/j.atherosclerosis.2015.04.038

Schoors, S., Bruning, U., Missiaen, R., Queiroz, K. C. S., Borgers, G., Elia, I., Zecchin, A., Cantelmo, A. R., Christen, S., Goveia, J., Heggermont, W., Goddé, L., Vinckier, S., van Veldhoven, P. P., Eelen, G., Schoonjans, L., Gerhardt, H., Dewerchin, M., Baes, M., ... Carmeliet, P. (2015). Fatty acid carbon is essential for dNTP synthesis in endothelial cells. *Nature*, *520*, 192–197. https://doi.org/10.1038/nature14362

Shah, G. N., Price, T. O., Banks, W. A., Morofuji, Y., Kovac, A., Ercal, N., Sorenson, C. M., Shin, E. S., & Sheibani, N. (2013). Pharmacological inhibition of mitochondrial carbonic anhydrases protects mouse cerebral pericytes from high glucose-induced oxidative stress and apoptosis. *The Journal of Pharmacology and Experimental Therapeutics*, *344*, 637–645. https://doi.org/10.1124/jpet.112.201400

Sharma, P. (2011). Inflammation and the metabolic syndrome. *Indian Journal of Clinical Biochemistry*, *26*, 317–318. https://doi.org/10.1007/s12291-011-0175-6

Shen, Y., Kapfhamer, D., Minnella, A. M., Kim, J. E., Won, S. J., Chen, Y., Huang, Y., Low, L. H., Massa, S. M., & Swanson, R. A. (2017). Bioenergetic state regulates innate inflammatory responses through the transcriptional co-repressor CtBP. *Nature Communications*, *8*, 624. https://doi.org/10.1038/s41467-017-00707-0

Soto-Heredero, G., Gómez de las Heras, M. M., Gabandé-Rodríguez, E., Oller, J., & Mittelbrunn, M. (2020). Glycolysis—A key player in the inflammatory response. *The FEBS Journal*, *287*, 3350–3369. https://doi.org/10.1111/febs.15327

Theodorou, K., & Boon, R. A. (2018). Endothelial cell metabolism in atherosclerosis. *Frontiers in Cell and Development Biology*, *6*. https://doi.org/10.3389/fcell.2018.00082

Toda, N. (2012). Age-related changes in endothelial function and blood flow regulation. *Pharmacology & Therapeutics*, *133*, 159–176. https://doi.org/10.1016/j.pharmthera.2011.10.004

Towler, M. C., & Hardie, D. G. (2007). AMP-activated protein kinase in metabolic control and insulin signaling. *Circulation Research*, *100*, 328–341. https://doi.org/10.1161/01.res.0000256090.42690.05

Tsuruda, T., Hatakeyama, K., Nagamachi, S., Sekita, Y., Sakamoto, S., Endo, G. J., Nishimura, M., Matsuyama, M., Yoshimura, K., Sato, Y., Onitsuka, T., Imamura, T., Asada, Y., & Kitamura, K. (2012). Inhibition of development of abdominal aortic aneurysm by glycolysis restriction. *Arteriosclerosis, Thrombosis, and Vascular Biology*, *32*, 1410–1417. https://doi.org/10.1161/ATVBAHA.111.237065

Wang, L., Cao, Y., Gorshkov, B., Zhou, Y., Yang, Q., Xu, J., Ma, Q., Zhang, X., Wang, J., Mao, X., Zeng, X., Su, Y., Verin, A. D., Hong, M., Liu, Z., & Huo, Y. (2019). Ablation of endothelial Pfkfb3 protects mice from acute lung injury in LPS-induced endotoxemia. *Pharmacological Research*, *146*, 104292. https://doi.org/10.1016/j.phrs.2019.104292

Wang, Y., Liang, Y., & Vanhoutte, P. M. (2011). SIRT1 and AMPK in regulating mammalian senescence: A critical review and a working model. *FEBS Letters*, *585*, 986–994. https://doi.org/10.1016/j.febslet.2010.11.047

Wellen, K. E., Hatzivassiliou, G., Sachdeva, U. M., Bui, T. V., Cross, J. R., & Thompson, C. B. (2009). ATP-citrate lyase links cellular metabolism to histone acetylation. *Science (New York, N.Y.)*, *324*, 1076–1080. https://doi.org/10.1126/science.1164097

Wong, B. W., Wang, X., Zecchin, A., Thienpont, B., Cornelissen, I., Kalucka, J., García-Caballero, M., Missiaen, R., Huang, H., Brüning, U., Blacher, S., Vinckier, S., Goveia, J., Knobloch, M., Zhao, H., Dierkes, C., Shi, C., Hägerling, R., Moral-Dardé, V., ... Carmeliet, P. (2017). The role of fatty acid β-oxidation in lymphangiogenesis. *Nature*, *542*, 49–54. https://doi.org/10.1038/nature21028

Wu, D., Huang, R. T., Hamanaka, R. B., Krause, M., Oh, M. J., Kuo, C. H., Nigdelioglu, R., Meliton, A. Y., Witt, L., Dai, G., Civelek, M., Prabhakar, N. R., Fang, Y., & Mutlu, G. M. (2017). HIF-1α is required for disturbed flow-induced metabolic reprogramming in human and

porcine vascular endothelium. *eLife*, *6*, e25217. https://doi.org/10.7554/eLife.25217

Wu, L., Zhang, L., Li, B., Jiang, H., Duan, Y., Xie, Z., Shuai, L., Li, J., & Li, J. (2018). AMP-activated protein kinase (AMPK) regulates energy metabolism through modulating thermogenesis in adipose tissue. *Frontiers in Physiology*, *9*. https://doi.org/10.3389/fphys.2018.00122

Xiong, J., Kawagishi, H., Yan, Y., Liu, J., Wells, Q. S., Edmunds, L. R., Fergusson, M. M., Yu, Z. X., Rovira, I. I., Brittain, E. L., Wolfgang, M. J., Jurczak, M. J., Fessel, J. P., & Finkel, T. (2018). A metabolic basis for endothelial-to-mesenchymal transition. *Molecular Cell*, *69*, 689–698. e687. https://doi.org/10.1016/j.molcel.2018.01.010

Xu, J., Yang, Q., Zhang, X., Liu, Z., Cao, Y., Wang, L., Zhou, Y., Zeng, X., Ma, Q., Xu, Y., Wang, Y., Huang, L., Han, Z., Wang, T., Stepp, D., Bagi, Z., Wu, C., Hong, M., & Huo, Y. (2019). Endothelial adenosine kinase deficiency ameliorates diet-induced insulin resistance. *The Journal of Endocrinology*, *242*, 159–172. https://doi.org/10.1530/joe-19-0126

Xu, Y., An, X., Guo, X., Habtetsion, T. G., Wang, Y., Xu, X., Kandala, S., Li, Q., Li, H., Zhang, C., Caldwell, R. B., Fulton, D. J., Su, Y., Hoda, M. N., Zhou, G., Wu, C., & Huo, Y. (2014). Endothelial PFKFB3 plays a critical role in angiogenesis. *Arteriosclerosis, Thrombosis, and Vascular Biology*, *34*, 1231–1239. https://doi.org/10.1161/atvbaha.113.303041

Xu, Y., Wang, Y., Yan, S., Yang, Q., Zhou, Y., Zeng, X., Liu, Z., An, X., Toque, H. A., Dong, Z., Jiang, X., Fulton, D. J., Weintraub, N. L., Li, Q., Bagi, Z., Hong, M., Boison, D., Wu, C., & Huo, Y. (2017). Regulation of endothelial intracellular adenosine via adenosine kinase epigenetically modulates vascular inflammation. *Nature Communications*, *8*, 943. https://doi.org/10.1038/s41467-017-00986-7

Yang, Q., Xu, J., Ma, Q., Liu, Z., Sudhahar, V., Cao, Y., Wang, L., Zeng, X., Zhou, Y., Zhang, M., Xu, Y., Wang, Y., Weintraub, N. L., Zhang, C., Fukai, T., Wu, C., Huang, L., Han, Z., Wang, T., ... Huo, Y. (2018). PRKAA1/AMPKα1-driven glycolysis in endothelial cells exposed to disturbed flow protects against atherosclerosis. *Nature Communications*, *9*, 4667. https://doi.org/10.1038/s41467-018-07132-x

Yeh, W. L., Lin, C. J., & Fu, W. M. (2008). Enhancement of glucose transporter expression of brain endothelial cells by vascular endothelial growth factor derived from glioma exposed to hypoxia. *Molecular Pharmacology*, *73*, 170–177. https://doi.org/10.1124/mol.107.038851

Zhang, M., Galdieri, L., & Vancura, A. (2013). The yeast AMPK homolog SNF1 regulates acetyl coenzyme a homeostasis and histone acetylation. *Molecular and Cellular Biology*, *33*, 4701–4717. https://doi.org/10.1128/mcb.00198-13

Zhang, Y., Qiu, J., Wang, X., Zhang, Y., & Xia, M. (2011). AMP-activated protein kinase suppresses endothelial cell inflammation through phosphorylation of transcriptional coactivator p300. *Arteriosclerosis, Thrombosis, and Vascular Biology*, *31*, 2897–2908. https://doi.org/10.1161/atvbaha.111.237453

Zu, Y., Liu, L., Lee, M. Y., Xu, C., Liang, Y., Man, R. Y., Vanhoutte, P. M., & Wang, Y. (2010). SIRT1 promotes proliferation and prevents senescence through targeting LKB1 in primary porcine aortic endothelial cells. *Circulation Research*, *106*, 1384–1393. https://doi.org/10.1161/circresaha.109.215483

SUPPORTING INFORMATION

Additional supporting information may be found in the online version of the article at the publisher's website.